Coatings **2012**, *2*, 8-44; doi:10.3390/coatings2010008

OPEN ACCESS

coatings

ISSN 2079-6412

www.mdpi.com/journal/coatings/

Article

Ion-Induced Surface Modification of Magnetically Operated Contacts

Karen Arushanov [1], Igor Zeltser [1], Sergey Karabanov [1], Rafail Maizels [1], Evgeny Moos [1] and Alexander Tolstoguzov [2,*]

[1] Ryazan Metal Ceramics Instrumentation Plant Joint Stock Company (RMCIP JSC), Novaya Street 51B, Ryazan 390027, Russian Federation; E-Mails: aka@akatel.ru (K.A.); zeltseria@rmcip.ru (I.Z.); smkarabanov@rmcip.ru (S.K.); maizelsrm@rmcip.ru (R.M.); e_moos@mail.ru (E.M.)

[2] Centre for Physics and Technological Research (CeFITec), Physics Department, Faculty of Sciences and Technology, Universidade Nova de Lisboa, Caparica 2829-516, Portugal

* Author to whom correspondence should be addressed; E-Mail: a.tolstoguzov@fct.unl.pt; Tel.: +351-21-294-85-76 (Ext. 10516); Fax: +351-21-294-85-49.

Received: 2 February 2012; in revised form: 15 February 2012 / Accepted: 15 February 2012 / Published: 24 February 2012

Abstract: A study has been made of permalloy (iron-nickel) contacts of reed switches before and after ion-induced surface modification using atomic force and optical microscopy, Auger electron and X-ray photoelectron spectroscopy. It has been found that the formation of surface nitride layers enhances corrosion and erosion resistance of contacts. We proposed to produce such layers directly into sealed reed switches by means of pulsing glow-discharge nitrogen plasma.

Keywords: reed switches; ion-plasma treatment; nitriding; atomic force microscopy; Auger-electron spectroscopy; X-ray photoelectron spectroscopy

---

List of Abbreviations

AES—Auger electron spectroscopy
AFM—atomic force microscopy
EEE—exoelectron emission

IPT—ion-plasma treatment
KPFM—Kelvin probe force microscopy
ME—mechanoemission
RT—room temperature
XPS—X-ray photoelectron spectroscopy

1. Introduction

One of the main technological processes of reed switch production is deposition of protective coatings on the surface of permalloy contacts (springs). To fabricate such coatings, electroplating of noble metals (gold, palladium, rhodium, ruthenium, *etc.*) is generally used [1]. However, this technique is characterized by large electro- and material consumption, high cost of equipment, low ecological standard, and by difficulty in depositing complex alloy coatings of well-controlled chemical and phase composition and structure. This is especially the case when thin nonporous films or thick films with low internal stresses and high adhesion ability are produced.

Surface modification by ion nitriding in pulsing glow-discharge plasma [2,3] is a very promising approach which improves the corrosion and erosion resistance of iron-containing alloys. This method generates surface nitrides and diffusion layers of specific structures. Depending on chemical composition, nitride layers on the surface of permalloy contacts can be either Fe_4N (γ'-phase) or $Fe_{2–3}N$ (ε-phase).

Our first application of pulsing glow-discharge nitrogen plasma for surface modification of reed switches was published in [4]; further developments and research are reported in [5–25].

The aim of the present work is to present an advanced study of how ion-plasma characteristics and switching conditions have an influence on the properties of permalloy contacts and, as a consequence, to develop a new technological approach for the ion-induced surface modification of reed switches.

2. Materials and Methods

2.1. Samples

Pilot samples were reed switches MKA-14108 made on the basis of commercially produced MKA-14103 contacts [1] (Figure 1). Pilot samples were fabricated without any special surface coatings.

Figure 1. Construction of pilot and standard reed switches.

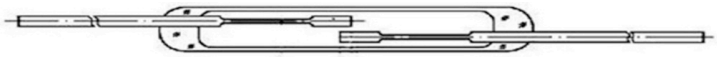

Reed switch with nano-structured contact surfaces of pieces

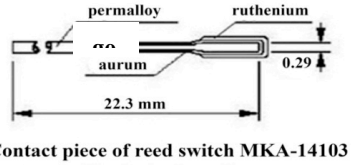

Contact piece of reed switch MKA-14103 with electrodeposit

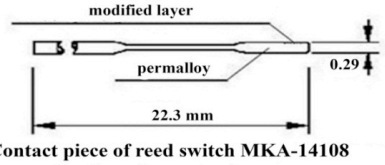

Contact piece of reed switch MKA-14108 after ion-plasma treatment

2.2. Technology

The manufacturing route of MKA-14108 production is shown in Figure 2. As against the standard technology, the operation *Plating* has been replaced by *Ion-Plasma Treatment* (IPT).

Figure 2. The manufacturing route of MKA-14108 production.

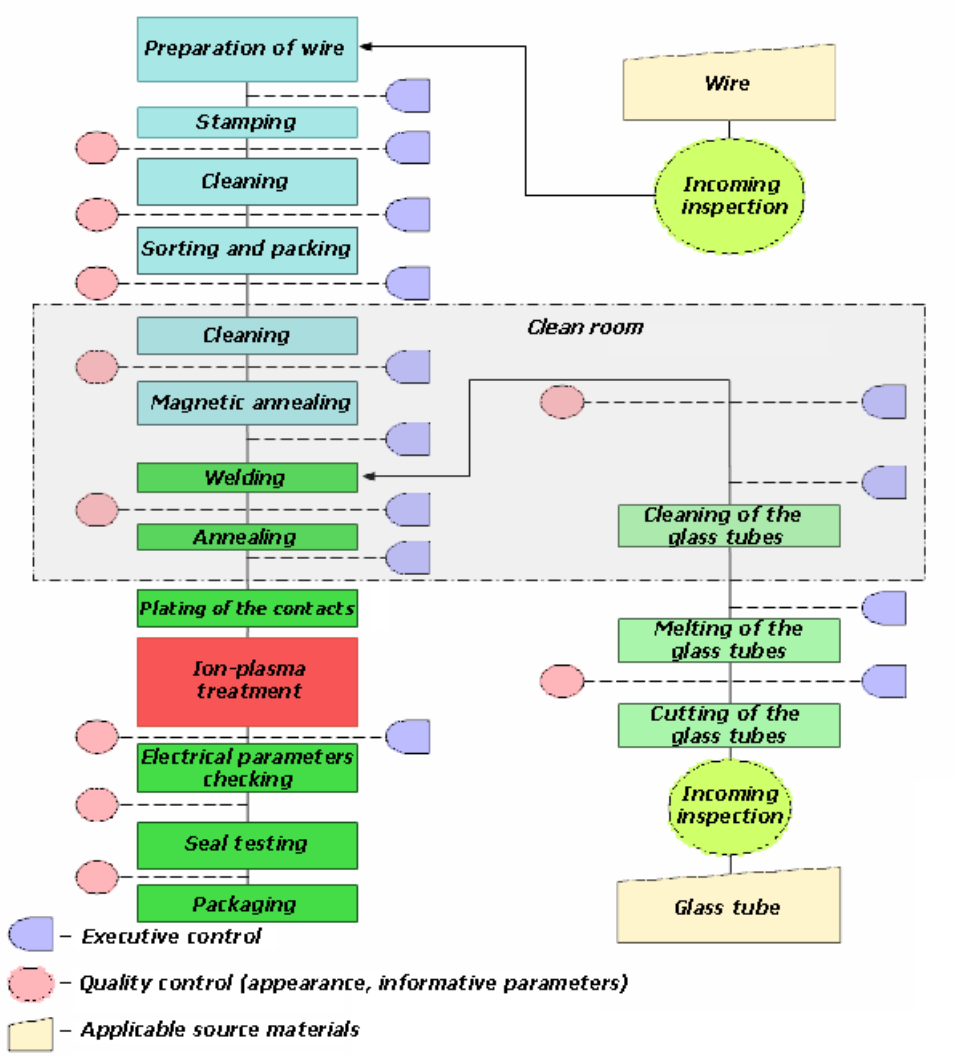

Contact springs were pressed of a vacuum-melt wire of permalloy Dilaton™ (Ni 52%, Fe 48%), then degreased and annealed in hydrogen. When sealing reed switches, spectroscopically pure (99.999%) nitrogen with the pressure in an envelope of (33–40) × 10^3 Pa was used as a filling gas.

2.3. Ion-Plasma Treatment (Ion Nitriding)

High-voltage pulsing discharge initiating between open contacts with a gap *d* of 27–30 μm was used for ion-plasma treatment [7]. Duration of a single IPT cycle was 30 s [4–6].

The distinctive feature of our approach as against the standard technology [2,3,26] is that ion nitriding of reed switches was carried out at a particularly high nitrogen pressure. In this case, there is no need for special vacuum equipment [2,26] since nitriding is performed directly into a sealed reed

switch. A glass envelope plays the role of a working chamber and contacts operate sequentially as anode and cathode.

Three characteristic regions with different surface topography were revealed on the contacts after IPT. One can recognize these regions in the images obtained by optical (Figure 3) and atomic force (Figure 4) microscopy.

Figure 3. Contact spring after hundredfold ion-plasma treatment.

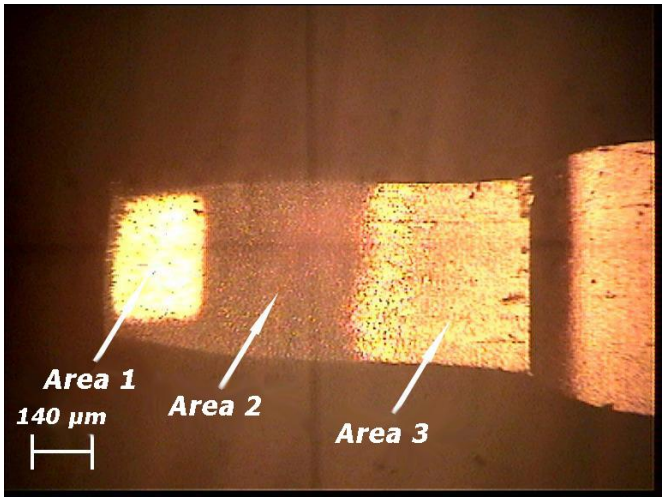

The region 1 (Figure 3 and Figure 4a, b) is the working area (contact overlapping zone), where gas discharge is initiated by high voltage pulses supplied to open contacts of a reed switch. As a result of the reactive cathode sputtering, FeN and NiN species are formed in the gas phase near the overlapping zone; part of which is deposited in the region 1, where surface nitriding has occurred according to the Kelbel mechanism [26].

Ion nitriding reactions taking place in Kelbel's glow discharge are schematically shown in Figure 5. In brief, nitrogen ions, after acceleration in the area of cathode drop bombard a target. The greater part of their energy (about 90%) is spent on heating, and the rest can provoke electron emission, ion implantation and sputtering of surface atoms (Fe, Ni, C, and O). Iron and nickel nitrides forming in the gas phase are deposited on the surface of contacts and on the wall of the glass envelope. When molecules of *Me*N (where *Me* is Fe and Ni) reach a hot (300–500 °C) permalloy surface, they dissociate and form low-order nitrides Me_nN, where n = 2–4. Escaping nitrogen diffuses into a target and evaporates in the plasma.

Due to diffusion, a part of FeN and NiN molecules deposits in the region 2 (Figure 4 and Figure 5c, d). Optical (Figure 3) and atomic force (Figure 4e, f) images show that the region 3 contains no nitrides or only a small amount of those. The heating of region 1 is produced by ion bombardment, and regions 2 and 3 are mainly heated via heat exchange between regions 1 and 2. Because of low temperature, the dissociation of FeN and NiN molecules, and, consequently, ion nitriding of these regions is a highly unlikely event. The products of reactive cathode sputtering form black coating in region 2 and on the inner wall of the glass envelope near to the overlapping zone (Figure 6). The same coating can be produced in region 1, if due to low ion energy (or current density) the temperature threshold of dissociation of FeN and NiN molecules is not exceeded. It is possible that a small amount of the cathode sputtering products diffuse to the back of contacts.

Figure 4. Atomic force microscopy (AFM) mapping of the contact surface of reed switch after 100-fold ion-plasma treatment (IPT): (**A**) two-dimensional (2D) and (**B**) tree-dimensional (3D) images of the region 1; (**C**) 2D and (**D**) 3D images of the region 2; (**E**) 2D and (**F**) 3D images of the region 3.

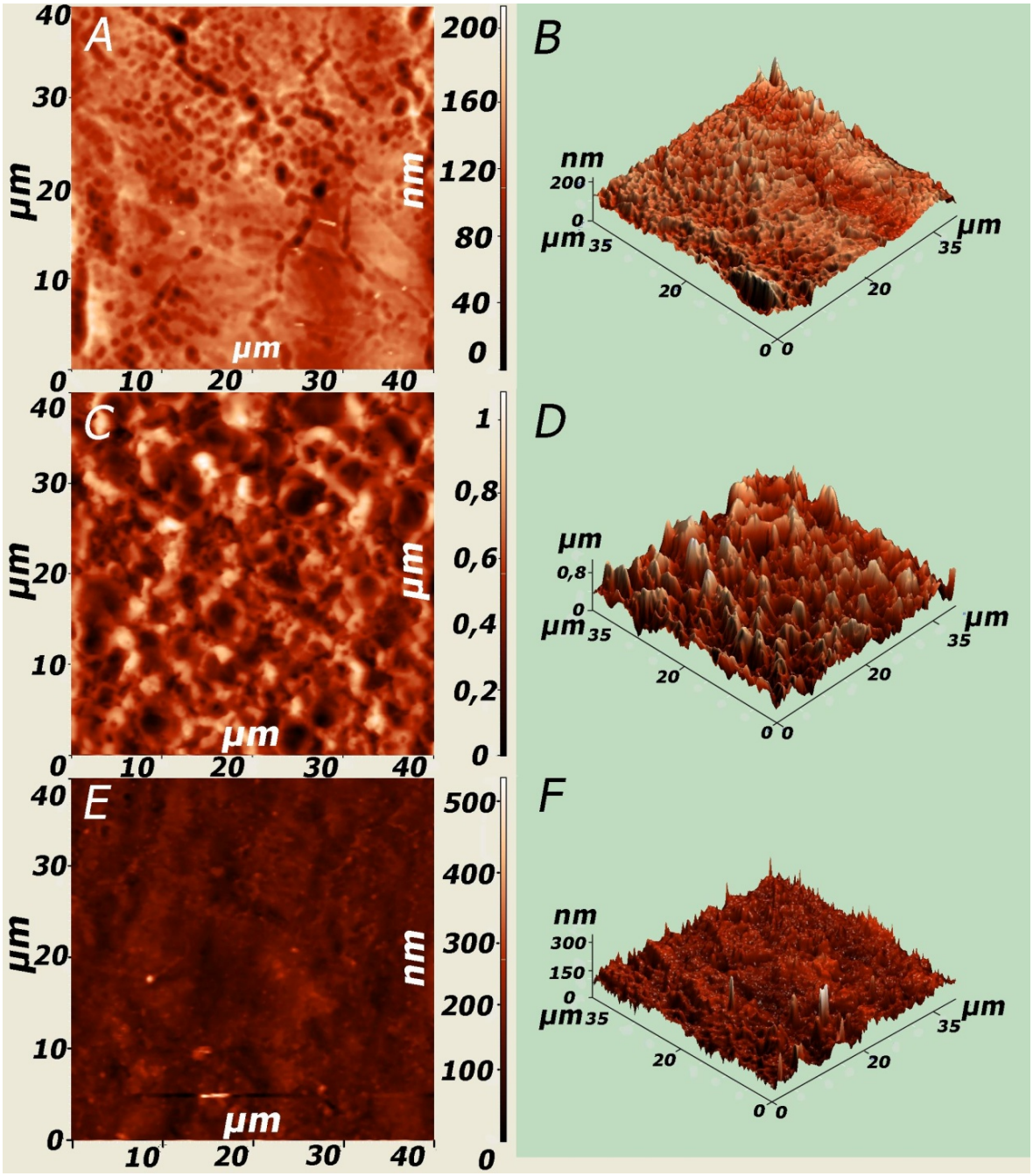

Figure 5. Ion nitriding reactions.

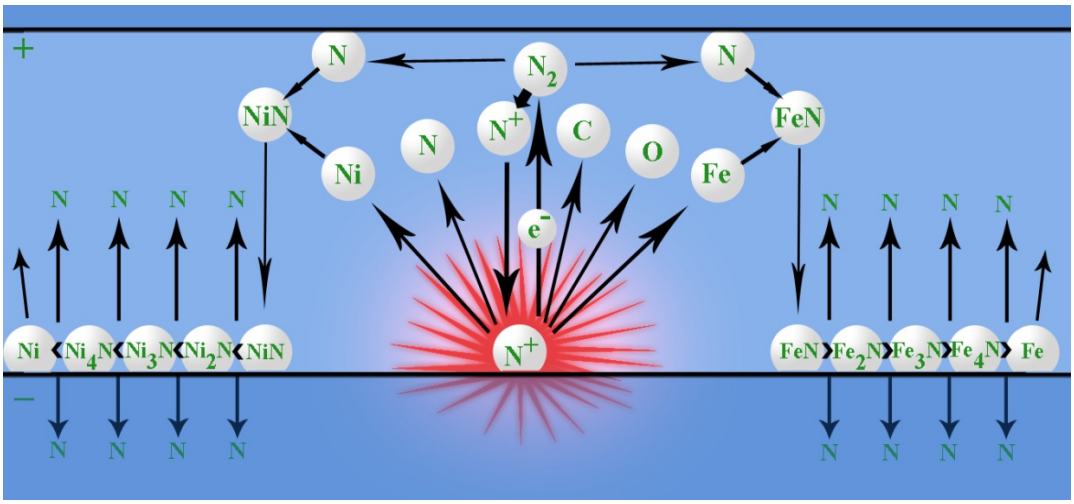

Figure 6. Reed switch after hundred-fold ion-plasma treatment.

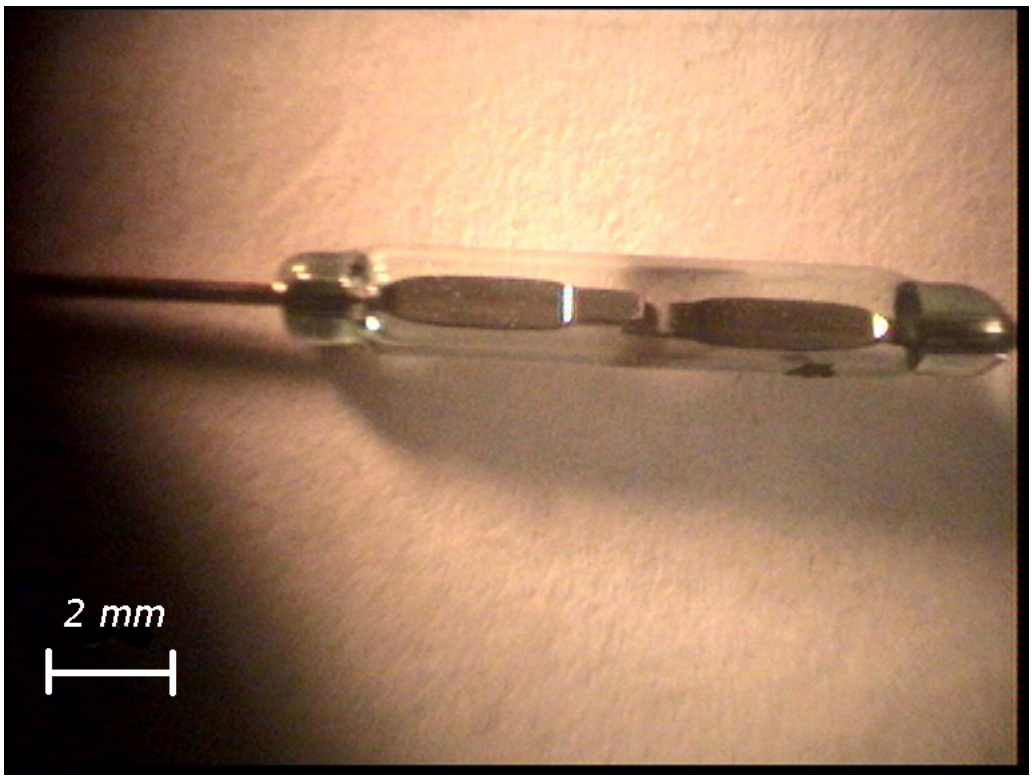

2.4. Testing and Research Methods

Both types of samples (after ion-plasma treatment and without) were put to the commutation tests. We measured electrical resistance, breakdown voltage and switching reliability using special-purpose equipment and methods described elsewhere [1].

A study of topography and local distribution of electrostatic potentials on the surface of contacts before and after ion-plasma treatment was made at ambient conditions by means of an atomic force microscope (AFM) using a Probe Nanolaboratory NTEGRA manufactured by NT-MDT (Zelenograd,

Russian Federation). For optical investigations we deployed a computerized metallurgical microscope MMP-4 by Asma (Kiev, Ukraine).

Elemental and chemical (phase) analyses were carried out by Auger electron spectroscopy (AES). We used a custom-built set-up with a cylindrical-mirror energy analyzer of the energy resolution 0.25%. The analyzer is equipped with an electron gun producing 1 μA beam of 100 μm in diameter (full width at half maximum). An ion gun with electron-beam ionization was used for sputter cleaning of the surface of contacts and for in-depth profiling. This gun generates an Ar^+ beam of a sample current density as high as 3.5 $mA \cdot cm^{-2}$; the ion-beam column possesses a differential pumping stage. Throughout the course of the experiments the pressure in the analytical chamber is maintained at the level of 2×10^{-7} Pa by means of oil-less ion and turbomolecular pumps.

Additional elemental and chemical surface analysis was carried out with a scanning X-ray photoelectron spectrometer (XPS) Quantera SMX by Physical Electronics (USA-Japan). All measurements were performed in an ultra-high vacuum 1×10^{-8} Pa without sputter cleaning of the surface of the contacts. We used an Al Kα 1486.6 eV X-ray beam of 7 μm in diameter.

Gas composition into glass envelopes was controlled by means of a custom-built magnetic mass-spectrometer with electron-beam ionization.

3. Results and Discussion

3.1. Degradation of Contacts

3.1.1. Influence of the Number of Switchings

Comparative switching tests in the "dry" electrical circuit (without any electrical load) of pilot reed switches MKA-14108 before and after IPT were performed. Each sample set included 100 pieces, and the maximal number of switchings was 10^7. The electrical resistance of the samples versus the number of switchings is presented in Figure 7.

The surface topography of contacts was studied by metallographic and atomic force microscopy (Figure 8–Figure 11).

With a growth of the switching number, the resistance of treated samples remains stable and does not exceed 0.1 Ohm (Figure 7, curve 2). On the contrary, the resistance of as-received (nontreated) samples exhibits 100 times gain and at $N = 3 \times 10^7$ reaches eight Ohms (Figure 7, curve 1).

At $N \sim 10^4$, dark brown spots appeared on the surface of nontreated contacts (Figure 8). These are the products of thermal decomposition of polymer films formed during switching. With a growth of N as high as 10^5, the size and darkening of these spots increased with simultaneous growth of R-value. In the range of 10^5–10^6 cycles, polymer films are totally decomposed, which results in decreasing electrical resistance. Further growth of the switching number (up to 10^7) leads to the formation of new polymer coatings accompanied by increasing R-value.

Figure 9–Figure 11 show that the growth of electrical resistance of nontreated contacts occurred also due to surface erosion (indicated by an arrow in the figures), *i.e.*, due to reduction of actual contact area.

Figure 7. Median value of the electrical resistance *R* of MKA14108 samples *versus* the switching number *N* in the "dry" circuit: 1—nontreated contacts, 2—contacts after IPT.

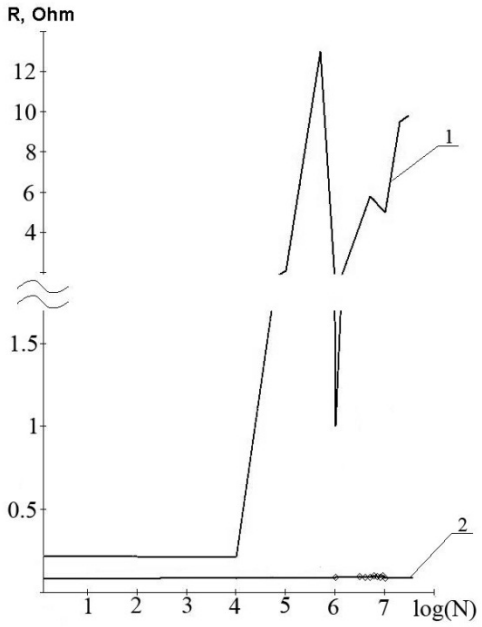

Figure 8. Modification of the contact surface after *N* switching cycles (300× optical magnification): (**a**) 10^4, (**b**) 10^5, (**c**) 10^6, (**d**) 10^7.

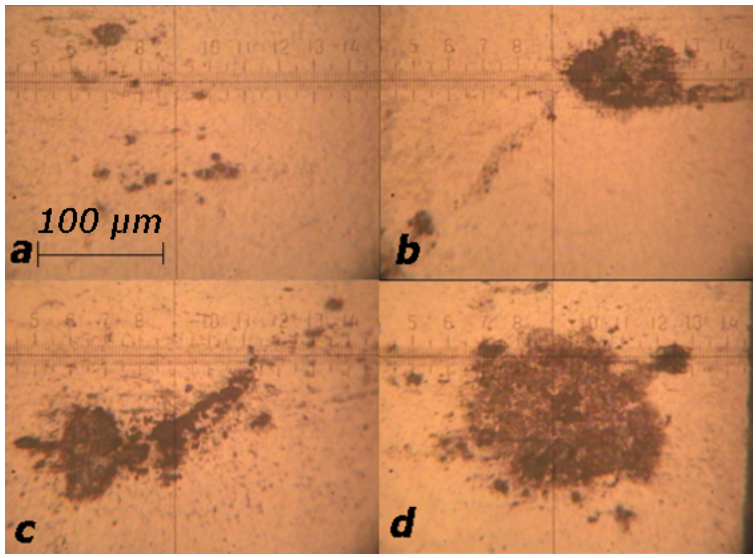

Conversely, the contact surface of treated springs was found to be more resistant to erosion processes due to a higher hardness of the nitride layers. As a result, in the course of the switching tests the electrical resistance of these contacts exhibits a low and stable value (Figure 7, curve 2).

The erosion of nontreated contacts is also influenced by the annealing temperature of wires used for contact fabrication and by the annealing conditions of contacts.

Figure 9. Surface mapping of nontreated spring after 5 × 10^5 cycles in the "dry" circuit: (**A**) optical image (300×), (**B**) 2D AFM image, (**C**) profile diagram along line 93, (**D**) 3D AFM image.

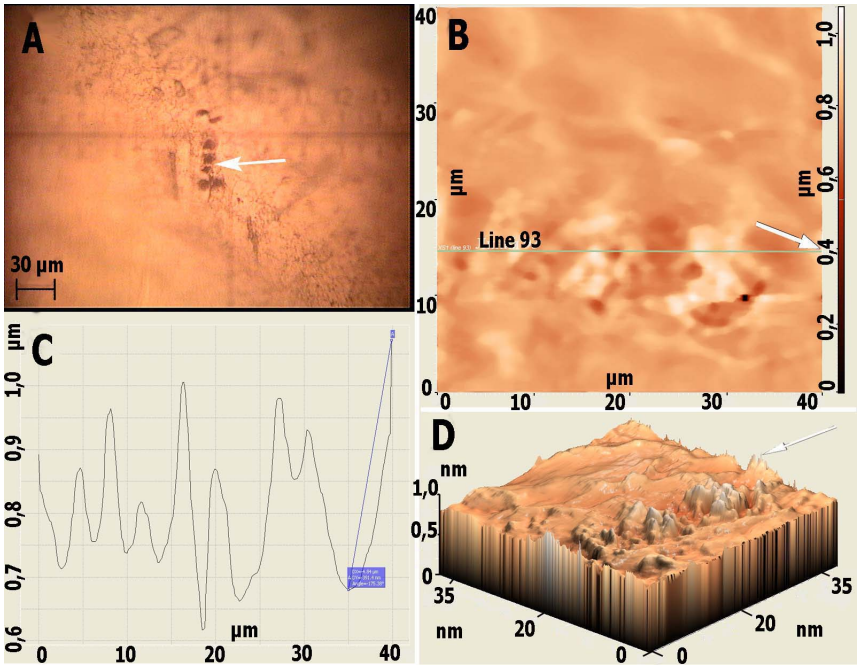

Figure 10. Surface mapping of nontreated spring after 10^6 cycles in the "dry" circuit: (**A**) optical image (300×), (**B**) 2D AFM image, (**C**) profile diagram along line 250, (**D**) 3D AFM image.

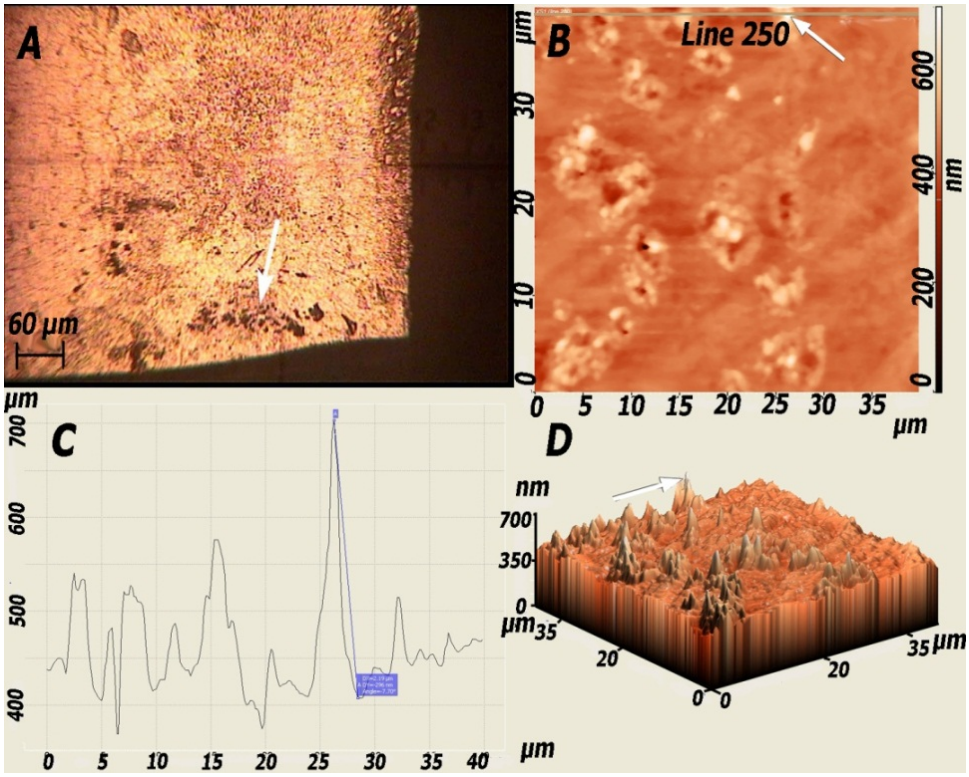

Figure 11. Surface mapping of nontreated spring after 5 × 10^5 cycles in the "dry" circuit: (**A**) optical image (300×), (**B**) 2D AFM image, (**C**) profile diagram along line 147, (**D**) 3D AFM image.

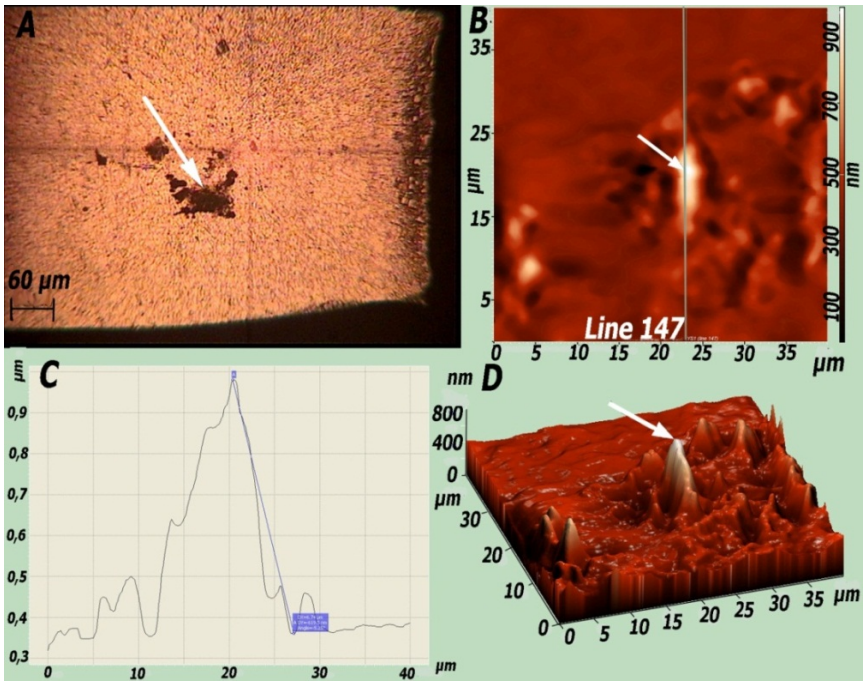

3.1.2. Effect of the Annealing Conditions

We have performed comparative switching tests for 6 sets of MKA-14108 samples distinguished from each other by the annealing temperature of the permalloy wire and the annealing conditions of the contacts (Table 1). The annealing of contacts was carried out in nitrogen (sets 1 and 4) and hydrogen (sets 2, 3, 5, and 6) atmosphere. Each set included 100 pieces, and the number of switchings in the "dry" electrical circuit was changed stage-by-stage from 0 to 10^7. At every test stage the *R*-value was measured (Figure 12).

From the experimental curves shown in Figure 12, one can see that the erosion of nontreated contacts is also influenced by the annealing conditions of the wire and contacts. The most favorable annealing conditions were realized for set 2.

We fitted the experimental data presented in Figure 12 by different polynomials [27]. In the wide time range, from 1 to 10^6 s, we used the logarithmic function:

$$R = a_0 + a_n \ln t^n \quad (1)$$

where *a* is the coefficient and *n* = 1–8 is the degree of polynomial. Over the range from 10^2 to 10^4 s, more appropriate was the power function:

$$R = (b_0 + b_m t^m)^2 \quad (2)$$

where *m* = 1–3. The results of our fitting are shown in Figure 13 and Figure 14.

Table 1. Annealing conditions of wire and contacts [1].

Set	Annealing temperature of wire (°C)	Annealing conditions of contacts
1	900	N_2 at 840 °C for 40 min
2	900	H_2 at 850 °C for 60 min
3	900	H_2 at 920 °C for 60 min
4	1050	N_2 at 840 °C for 40 min
5	1050	H_2 at 850 °C for 60 min
6	1050	H_2 at 920 °C for 60 min

Figure 12. Median value of the electrical resistance *R* of nontreated MKA14108 samples versus the number of switching cycles *N* for different sample sets.

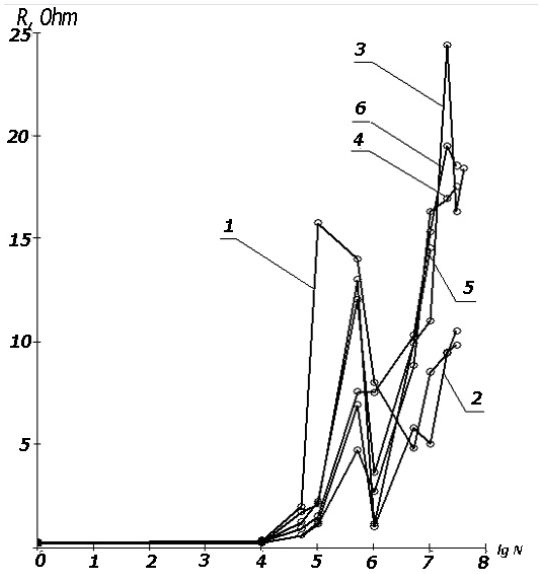

Figure 13. Fitting curves obtained with Equation 1 for the electrical resistance *R* of nontreated MKA14108 samples versus the duration of the experiment *t* at 100 Hz for different sample sets (curve 7 shows the averaged data for the sets 2, 3, 4, and 6).

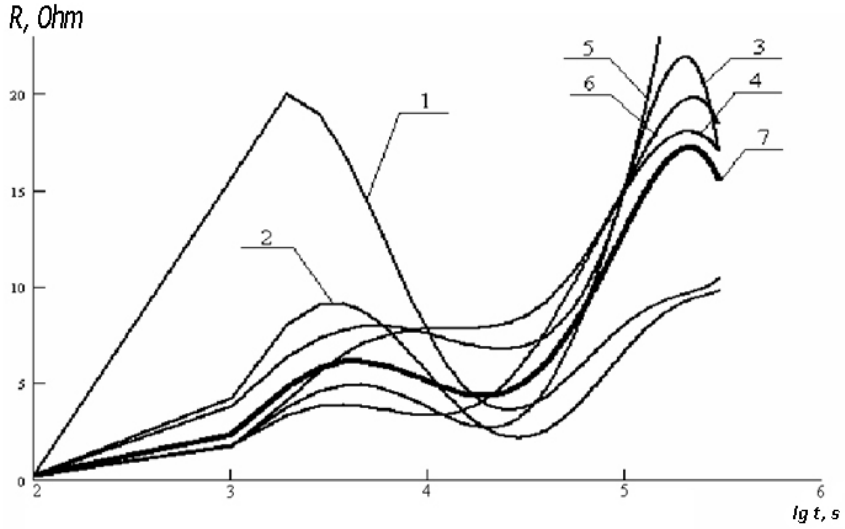

We used the data presented in Figure 13 to estimate the nonfailure operating time of reed switches.

3.1.3. Dynamic Noise

Dynamic noise, *i.e.*, an electrical potential arising between contacts under switching in the "dry" circuit, was measured using the experimental set-up schematically presented in Figure 14. Mechanical oscillations of contacts were initiated by a sinusoidal wave generator at 50, 100 and 500 Hz.

Figure 14. Schematic view of the experimental set-up: G—sinusoidal wave generator, R.S—reed switch, L—inductor, C—oscillograph.

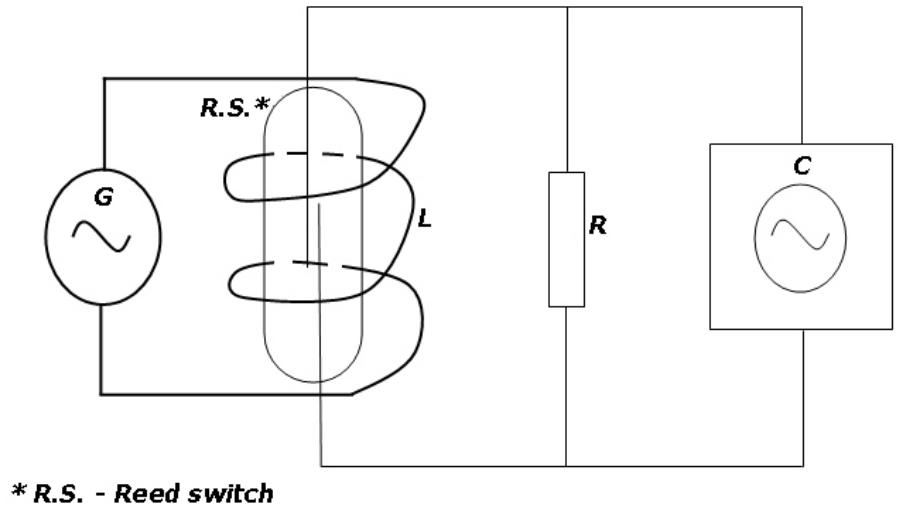

We found that the amplitude of dynamic noise increased from 10 to 30 mV with a growth in the commutation rate. The influence of this noise on the erosion of contacts is discussed below.

It has long been known (see, e.g., [28] and references cited therein) that ferromagnetic material in an unmagnetized state consists of a large number of saturated magnetic domains. Under the actions of magnetic field, mechanical stresses and temperature (all these factors are present in our case) the magnetic state of the ferromagnetic is changed; that is accompanied by the movement of domains towards a new equilibrium state, more efficient in terms of energy. Such movement includes both reversible and irreversible displacement of domain walls and rotation of the spontaneous magnetization vectors. According to Faraday's law of electromagnetic induction, an alternating electromagnetic field is generated in the bulk of ferromagnetic along with uncompensated surface electric potential.

This dynamic potential depends on the type of influences on ferromagnetic, and if the magnetization is changed under the action of an external magnetic field H initiating the magnetic induction B in the sample, the potential is proportional to B, *i.e.*, $E \sim \frac{\partial B}{\partial t}$.

For ferromagnetic with nonvanishing magnetostriction, the magnetization is changed under the influence of mechanical stresses $\sigma(x,t)$, and the potential Φ can be represented by

$$\Phi = k\sigma(x,t)\left(\frac{\partial B}{\partial t}\right)_{H=const} \quad (3)$$

where k is the coefficient of proportionality.

The domain structure of ferromagnetic can be changed under pulsed heating; that also generates surface electric potential.

The surface potential is very sensitive to switching conditions (magnetic, mechanical, and thermal). Since each of the contacts has its own specific domain structure, it leads to the appearance of a potential difference between them. Usually, this difference is within the range from tens of microvolts to a hundred millivolts; its value depends on the strength of action and on the materials used for contact fabrication

It is known [29] that by touching two metals with different electron work functions $e\varphi_1$ and $e\varphi_2$ ($e\varphi_1 < e\varphi_2$), electrons from the Fermi level of the metal with the work function $e\varphi_1$ can pass through the potential barrier into the empty states of the metal with the larger work function $e\varphi_2$. It results in the contact potential difference equal to ($e\varphi_2 - e\varphi_1$). Since the contact surfaces are rather heterogeneous in terms of work function, the contact potential difference between them during disconnecting can reach several volts.

Due to friction effects, polymer films can be polarized [29] and this also produces a potential difference between contacts covered by such films. Moreover, active and weakly-connected dielectrics can be moved in the overlapping zone. The moving force F depends on the field nonuniformity at the boundary of dielectrics and contacts. Using the energy conservation law one can estimate this force as [30]:

$$F = \frac{U^2 \varepsilon \varepsilon_0 w}{2l} \quad (4)$$

where w is the width of the overlapping zone, l is the thickness of dielectric film, ε_0 is the dielectric constant of the vacuum, ε is the relative permitivity of the dielectric, U is the electrical potential between contacts.

Thus, dielectric films and particles are able to migrate under the action of an F-force in the zone of contact overlapping and to interfere with the closure of contacts.

Exoelectron emission (EEE) and mechanoemission (ME) can also activate directional mass transfer on the surface of contacts working in the "dry" electric circuit. EEE is one of the possible channels for relaxation of excited states generated in the near-surface region of 100–1000 Å. All processes of restoration of existing surface equilibrium or of reaching new equilibrium conditions are accompanied by energy release that can cause the emission of exoelectrons with an average energy within the range from tenths eV to 1 eV [29].

ME is an emission of energetic charged particles and photons due to the break-down of polymers adhesive bonds or destruction of dielectric materials. The emission intensity depends on the rate of crystal destruction or breaking of the adhesive bonds as well as on the structure and chemical composition of the contacting surfaces. The energy of the emitted electrons is within 1–100 keV [29].

Destruction and tearing polymer films off the contact surface can occur during the switching tests. This results in the formation of cracks with charged walls, *i.e.*, generation of highly intensive electric fields. Simultaneously, the destroyed materials are evaporated as neutrals and ions, and dissolved gasses are emitted; this provokes electron emission and discharge ignition within cracks. The perturbance of the surface layers of contacts along with defect and radical recombination can also lead to EEE.

Many processes discussed above can produce potential difference between contacts. However, to estimate their concrete action on the erosion of permalloy contacts is a rather difficult task.

From the voltage oscillograms one can see that after the contact breaking the generated voltage is about tens millivolts. Using the formula for a parallel-plate capacitor, we can estimate the interelectrode spacing d and electric field intensity E:

$$d = \frac{\varepsilon\varepsilon_0 SU}{q} \tag{5}$$

$$E = \frac{U}{d} \tag{6}$$

where S is the area of the plate, and q is the charge of the capacitor.

This charge can arise, for instance, during contact due to the difference in work functions of the contacting materials. Under the influence of elastic forces formed in contacts due to their bending, contacts move away from each other. Meanwhile, at a certain distance between contacts, the discharge of a capacitor takes place, and after that the contacts become again electrically neutral. Then, under the action of a magnetomotive force excited by the passing of an alternating current through a solenoid coil, the contacts close again; which results in the charging of the capacitor, *etc.* In the course of discharge via field desorption or vacuum breakdown, directional mass transfer takes place. If only singly charged ions from the cathode material are transferred, their quantity N_1 realized in every switching cycle is equal to the charge of the capacitor.

According to our microscopic data, after 3×10^7 switchings the microasperity exhibits the shape of a taper (cone) with a height H = 1 μm and a radius of the cone base R = 8 μm (Figure 11c). One can estimate the total amount of material N transferred during the whole period of switching

$$N = \frac{\pi R^2 H \rho N_A}{3M} \tag{7}$$

where ρ is the density of material, N_A is the Avogadro constant, M is the molecular weight.

For iron, ρ = 7.8 g·cm^{-3} and M = 55.847. In the case of permalloy, N is equal to 5.63×10^{12} atoms. For single switching $N_1 = N/k = 1.87 \times 10^5$, where k is the total number of switchings (in our case $k = 3 \times 10^7$). Using Equation 5 and Equation 6 with ε = 1, $\varepsilon_0 = 8.85 \times 10^{-12}$ F·m^{-1}, $S = 10^{-6}$ m^2, $q = 1.87 \times 10^5 e$ (the elementary charge $e = 1.602 \times 10^{-19}$ C), U = 0.03 we estimated d = 1 nm and $E = 0.34 \times 10^7$ V·cm^{-1}.

For an electric field of $E > 10^5$ V·cm^{-1} the microroughness of the cathode surface greatly influences the discharge ignition since the E-value can grow at a hundred times on the summit of an asperity. It results in local electron emission and can initiate a microexplosion of asperities. For example, if the field intensity into a gas-filled gap reaches 10^6 V·cm^{-1}, it can be in the range of 10^8 V·cm^{-1} on an apex. In this case, the microexplosion of the tungsten apex is realized during 10^{-9} s with plasma initiation consisting of cathode material; that amplifies the electron emission from the cathode. In our case U =30 mV and the electric field E can reach 0.3×10^7 V·cm^{-1} if the gap between contacts becomes 0.1 nm; it then makes the explosion of microasperities possible.

3.1.4. Processes Leading to Erosion of Contacts

To analyze the processes leading to erosion of contacts under switching in the "dry" electric circuit, we examined the time diagram of the reed switch operation (Figure 15).

Figure 15. Time diagram of reed switch operation.

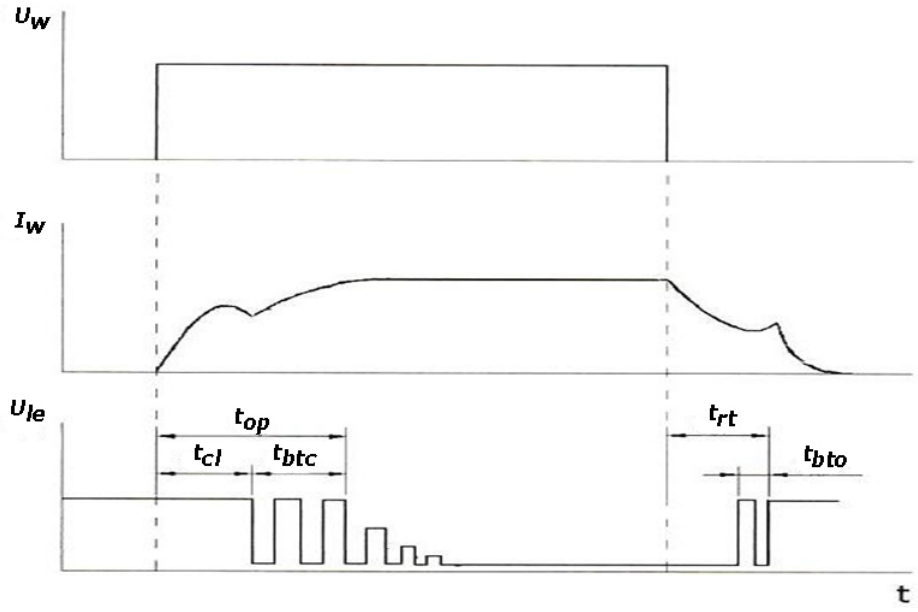

In this figure, U_w, U_{le} are the potentials of control winding and reed switch contacts, respectively; I_w is the current of the control winding; t_{cl} is the contact time, *i.e.*, an interval from the beginning of the action of controlling the magnetic field to the first contact of the reed switch; t_{op} is the operating time, *i.e.*, the interval from the beginning of the action of controlling the magnetic field to the last contact of the reed switch; t_{btc} is the contacting bounce time, *i.e.*, an interval from the beginning of the first to the beginning of the last contact of the reed switch; t_{rt} is the release time, *i.e.*, an interval from the beginning of reduction of controlling the magnetic field to the last breaking of contacts; t_{bto} is the breaking bounce time, *i.e.*, the interval from the beginning of the first to the beginning of the last breaking of contacts.

3.1.4.1. Lattice Imperfection

Under the influence of a pressing force both plastic and elastic deformations of the contacting surfaces occurred. In the case of plastic deformation, most part of the work carried out during deformation turns into heat, and the rest is accumulated in the metal as an additional energy. The accumulation mechanisms relate to the changing of the metal structure; vacancy and dislocation concentrations are growing, which leads to the growth of resistivity of the near-surface layers.

During switching the additional energy is not only accumulated but also released in the processes of recovery and recrystallization.

As a result of plasto-elastic deformation, point defects are additionally generated on the surface of contacts. The shearing greatly increases a number of dislocations: the dislocation density ρ of the

unstrained metal is usually is the range from 10^6 to 10^8 cm^{-2}, but under deformation of 80–90% it reaches 10^{11}–10^{12} cm^{-2}.

It has been shown [31] that mechanical stress and thermal motion increase the concentration of vacancies

$$n = n_0[1 + wt\, exp(\alpha\sigma)] \quad (8)$$

where n_0 is the initial vacancy concentration, w is the probability per unit time t to generate a new vacancy due to atom disordering, σ is the active mechanical stress, and

$$\alpha = \frac{0.5qV_a}{RT} \quad (9)$$

where q is the coefficient characterizing stress density in the defect region, V_a is the atomic volume, R is the molar gas constant, T is temperature. According to [31–35], under the action of constant mechanical stress, deformation rate and temperature the vacancy concentration exhibits linear growth versus deformation time.

Sharp growth of lattice imperfection occurring in the plastic strain range has an influence on the physicochemical properties of the surface and near-surface layers of the contacts. For instance, intensified surface adsorption stimulates the generation of dielectric and (or) semiconductor films on the contact spots, *i.e.*, increases the transient resistance of the reed switch.

3.1.4.2. Radicals

During switching the contacting surfaces become partly saturated with chemical radicals formed via mechanical destruction of complex molecules [36]. Besides, under the plastic deformation of surface layers, a great number of dislocations and seed cracks is produced that also stimulates radical generation at later steps of the manufacturing route [33–35].

Under local heating of contacts, radicals intensively interact with the treated surface. Most of them penetrate into surface layers making them harder; some part is oxidized, forming surface polymer films, or evaporated into the gas-filling volume of the reed switch.

These processes need complex molecules with a linear structure, which can decompose to a large amount of fragments also possessing linear structure. Carbon dioxide (CO_2) is such a molecule; according to our mass spectrometric measurements it formed with hydrogen or alone in a quantity of 2–5% in the gas volume of the reed switches after sealing and (or) switching tests.

3.1.4.3. Gas Release

Gas emission from solid-state materials under mechanical stress and following destruction was studied in [37,38]. The volume of released hydrogen was measured versus the intensity of the mechanical stress. It was shown that the quantity of hydrogen increases in the plastic strain range reaching the maximum at the moment of sample destruction. The main peculiarities of gas release under mechanical stress are general for different metals, and they are observed at the switching of the contacts.

3.1.4.4. Chemical Reactions

During sealing or switching heating of contacts occurred. The structure and properties of the contacting surfaces depend on interaction between the gas atmosphere and the permalloy. Carbon dioxide and water vapor are gas species, which not only oxidize but also decarbonize iron alloys. The main source of water vapor is the surface of the glass envelope; carbon and hydrogen are evaporated from the contacts.

The principal reactions of oxygen interaction with iron and iron oxides are in the order

$$2Fe + O_2 = 2FeO \quad (10)$$

$$3Fe + 2O_2 = Fe_3O_4 \quad (11)$$

$$4Fe + 3O_2 = 2Fe_2O_3 \quad (12)$$

The following reactions are also possible

$$4FeO + O_2 = 2Fe_2O_3 \quad (13)$$

$$4Fe3O4 + O_2 = 6Fe_2O3 \quad (14)$$

Water vapor interacts with iron and iron oxides at a temperature lower than 570 °C as

$$2Fe_3O_4 + H_2O = 2Fe_2O_3 + H_2 \quad (15)$$

$$3Fe + 4H_2O = Fe_3O_4 + 4H_2 \quad (16)$$

At higher temperature, in addition to reaction 16 the following reactions are possible

$$3FeO + H_2O \Leftrightarrow Fe_3O_4 + H_2, \quad (17)$$

$$Fe + H_2O \Leftrightarrow FeO + H_2 \quad (18)$$

As regards carbon dioxide, at temperatures lower than 570 °C it reacts with iron oxides as

$$2Fe_3O_4 + CO_2 \Leftrightarrow 3Fe_2O_3 + CO, \quad (19)$$

$$3FeO + 4CO_2 \Leftrightarrow Fe_3O_4 + 4CO \quad (20)$$

At temperatures higher than 570 °C, in addition to reaction 20 the following reactions can take place

$$3FeO + CO_2 \Leftrightarrow Fe_3O_4 + CO, \quad (21)$$

$$Fe + CO_2 \Leftrightarrow FeO + CO \quad (22)$$

In a complex gas atmosphere consisting of carbon monoxide and dioxide, hydrogen and water vapor, the components can also interact with each other

$$CO + H_2 \Leftrightarrow C + H_2O, \quad (23)$$

$$CO + H_2O \Leftrightarrow CO_2 + H_2 \quad (24)$$

3.1.4.5. Vacuum Breakdown

Usually, microasperities within the range of 0.01–0.1 μm in height exist on the surface of contacts [1,38–40]. These irregularities are located on the extensive wavy base with a period of 10^3–10^4 μm and a height of 1–10 μm [41]. Such roughness and corrugation allow physical touch of contacts only at some points.

During switching the contacting surfaces become deformed by a pressing force, especially, in the area of the microasperities. The stronger the pressing force the greater the number of microasperities which change their form and electrical conductivity [38,39].

Vacuum breakdown occurs at the distance of the critical approach of contacts as discussed in [9,42,43]. After contact, the force leading to withdrawal of the springs appears. This force is caused by spring elasticity, high metal vapor pressure and plasma density due to microexplosions occurring in the contacting areas [41].

3.1.4.6. Adhesion

It was shown [44] that during contacting-disconnection of an AFM probe with a sample surface some outgrowths of adhesive nature are formed along with breaking of contact bridges. Very probably similar process can occur in reed switches during their operation in the "dry" electric circuit. Due to breaking of contact bridges the formation of nanoasperities on the contacting surfaces is possible, already at the first stage of contact disconnection.

3.1.4.7. Dynamic Noise and Bridge Erosion.

During contact bounce (chatter) the potential difference between contacts can reach 10–30 mV. This voltage is produced by electroinduction in the ferromagnetic material on rearrangement of its domain structure under the influence of the mechanical stress and magnetic field [28]. We estimated the energy accumulated in the bounce period in the capacitor formed by reed switch contacts is in the range of 10^{-11} to 10^{-16} J. It is quite sufficient to melt nanoasperities existing on the contact surfaces, since according to our calculation the heat of melting of a single iron nanoasperity of a cylindrical form is ca. 0.5×10^{-18} J.

The current density is non-uniform over the surface of contacts due to the aforementioned surface irregularities. During disconnection of the contacts bridges of molten metal can be formed in these areas due to intense local ohmic heating; subsequent explosions of these bridges lead to strengthened erosion of contacts.

3.1.4.8. Magnetostrictive Triboeffects.

During disconnection the closed contacts undergo a magnetostrictive shift. The most part of the work carried out during this shift is against friction forces and turns into heat. Our calculations show that the released energy (ca. 10^{-9} J) is also enough to melt the surface nanoasperities.

We estimated the chemical affinity A under magnetostrictive sliding friction in an open tribosystem, in which all mechanical activities give rise to only tribochemical reaction, as [44,45]:

$$A = -\frac{\mu N_A P \sigma_0 \delta}{\eta \sigma} \quad (25)$$

where μ is the friction factor, P is the physical load, σ_0 is the actual contacting spot area of the atom or molecule, δ is the diameter of the contacting microroughness along which the state of the activated complex is safe under sliding of objects, η is the part of rated area that comes into actual contact, σ is the rated contacting spot area of the interacting objects.

In our case we obtained $|A| \sim 2.65 \times 10^7$ J·mol^{-1}. It means that the magnetostrictive friction is able to activate many nonspontaneous processes including complete decomposition of any chemical compounds and triboplasma generation.

If a contact is fabricated of quite soft and low-melting metal (like permalloy as against ruthenium) without corrosion- and erosion-resistant coatings, one can expect melting of the surface nanoasperities along with speeding-up of diffusion processes, especially, in the case of triboplasma generation. Consequently, due to the formation of specific surface relief the actual contacting area decreases and its transient resistance increases. All these processes are observed for untreated (by plasma) iron-nickel contacts without special coatings.

3.1.4.9. Acoustic Vibrations

It has been established [46–50] that acoustic vibrations under magnetostrictive friction have an effect on the tribosystem similar to additional mechanical load.

Damping of acoustic vibrations reduces such loading and, as a result, decreases damaging and improves the wear resistance of materials [49–53]. Using pulsed electrical discharge we produced the thin ion-modified surface region with specific physical-mechanical properties differing from the properties of the bulk material. Such a region has an influence on the propagation of surface acoustic waves, which become localized into a layer of thickness equal to the wave-length.

3.2. AFM Diagnostics [54]

We used Si-made cantilevers NSG10/W_2C covered by a hard conducting 30 μm W_2C film with work function $e\varphi_p$ = 4.902 eV. In the Kelvin mode (Kelvin probe force microscopy) the contact potential difference $\Delta\varphi(x, y)$ between the apex of the probe and the sample surface is estimated as

$$\Delta\varphi = \varphi_p - \varphi_s \tag{26}$$

where φ_s is the potential of the sample surface.

According to [29], the work function can be represented by the sum of internal $e\varphi_{int}$ and external $e\varphi_{ext}$ parts

$$e\varphi_s = e\varphi_{int} + e\varphi_{ext} \tag{27}$$

Due to partial spreading of electron clouds out of the metal, a double dipole layer, negatively charged outside, is formed on the gas (vacuum)-metal interface. To overcome this layer with d thickness an electron should perform work equal to $e\varphi_{ext}$ against the force of the electrostatic field E. In this case, the work function $e\varphi_{ext}$ is calculated as [29]

$$\varphi_{ext} = Ed = 4\pi\sigma d = 4\pi P \tag{28}$$

where σ is the effective charge density of the capacitor, and P is the dipole moment normal to the surface.

From Equation 28 it follows that different numbers of $\Delta\varphi(x, y)$ obtained by the Kelvin method can be explained via the difference in the spreading of the electron clouds. The relief and composition of the surface investigated as well as the type of crystal face have an influence on such processes [29]. At

ambient conditions, absorption greatly affects the work function and the spreading of the electron cloud, and the data obtained in air differ from those measured under vacuum conditions.

3.2.1. Nanorelief with Asperities of Higher Conductivity

AFM mapping of the nitrided contact surface is shown in Figure 16. One can see alternating dark and light round-shaped areas arising due to the difference in height of the surface relief. More detailed relief information can be obtained from the image measured with a lower scanning area (Figure 17).

Figure 16. AFM image of the nitrided contact surface (the scanning area is 7 × 6 μm^2).

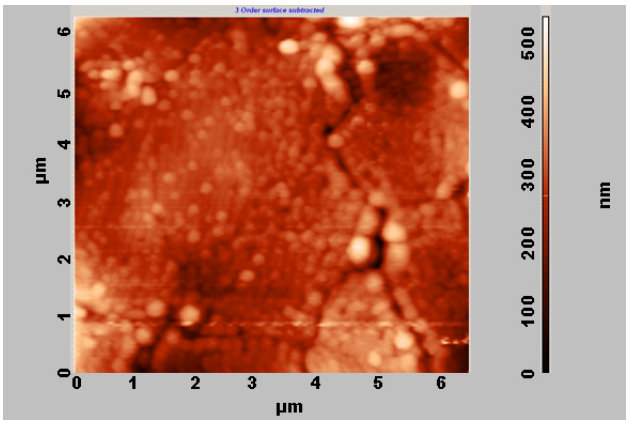

Figure 17. (**a**) AFM image of the nitrided contact surface (the scanning area is 2 × 2 μm^2); (**b**) profile diagram along line 175; (**c**) statistical distribution of the heights.

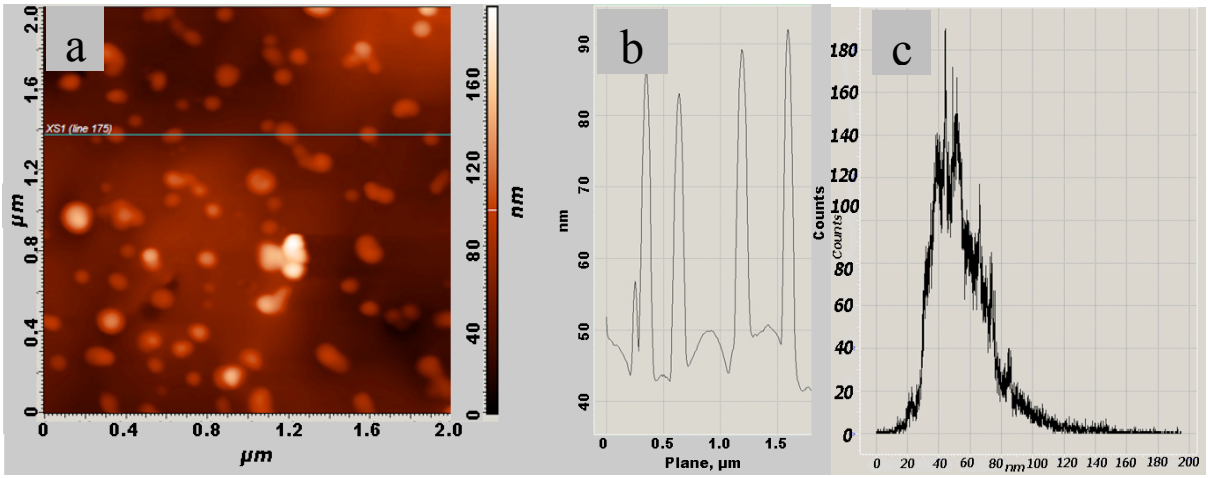

Statistical analysis (Figure 17c) indicates that the average height of asperities is ca. 50 nm. The lateral dimensions of asperities at the bottom are in the range of 70–100 nm, and their width at mid-height is about 70 nm.

The spreading resistance images of the contact surface, collected after ion-plasma treatment (Figure 18b), demonstrate the specific conducting properties of nanoasperities. To the best of our knowledge the formation of such nanostructures on a permalloy surface after ion-plasma treatment has not previously been reported.

Figure 18. AFM images of the nitrided contact surface: (**A**) constant force mode, (**B**) method of spreading resistance imaging.

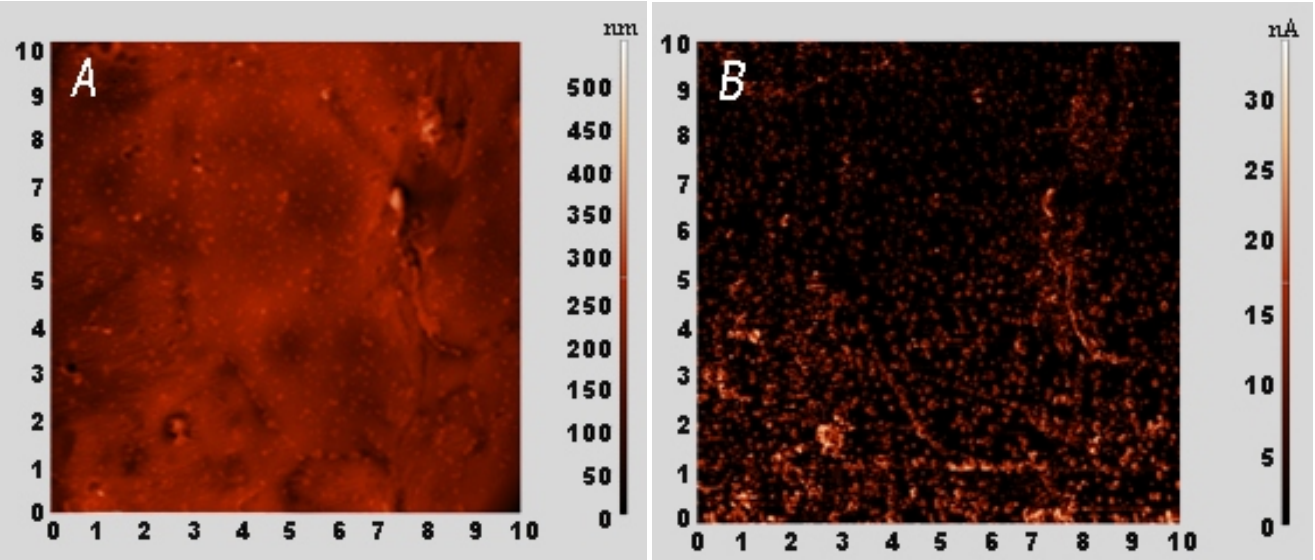

As mentioned before, contacting in reed switches always occurs at some points (spots) randomly distributed on the surface of the contacts; it is impossible to produce a reed switch, in which contacting is carried out over the whole surface of the spring. During the manufacturing route, especially with galvanic plating (electrodeposition), foreign dielectric particles can be deposited on the surface of the contacts. As a result, the transient resistance exhibits a growth due to formation of a gap between the springs, and the number of contacting spots is greatly reduced.

It has been shown [55,56] that gradient fields, as well as laser and ion irradiation produce imperfection-strain instabilities on the surface of condensed materials. It can result in the development of different surface structures. In the case of ion-plasma treatment of contacts, the combination of field and temperature gradients, the intensity and duration of nitrogen ion-bombardment along with some other factors, make surface relief in the form of nanostructured asperities.

3.2.2. Surface Pores and Cones

Ion-plasma treatment modifies the energy state of contacts that leads to the evolution of surface relief, mainly due to heterogeneous etching, ion-induced segregation and desorption. As a result, ion-induced mechanical strains, recrystallization processes, changes of chemical composition, dislocation mobility and phase state are revealed in the near-surface layers.

We found that IPT produces surface pores in region 1 (see Figure 5a, b and Figure 19). With increasing IPT duration, the concentration of these pores grows. After some time, the conical asperities begin to develop at the bottom of the pores (Figure 20).

Figure 19. AFM image of the region 1 after 200-fold IPT.

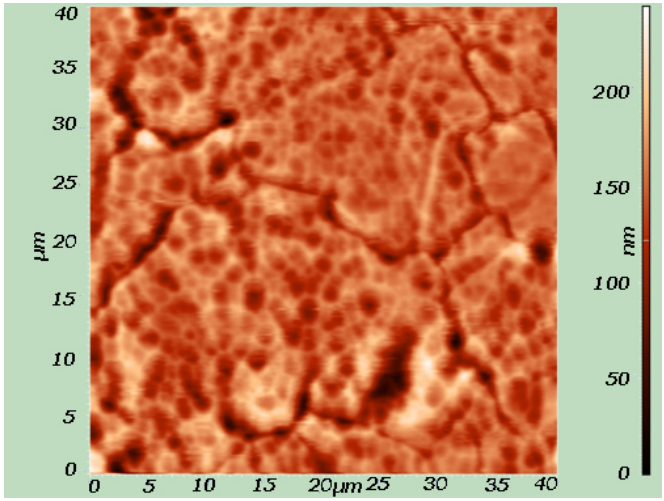

Figure 20. 2D (**A**) and 3D (**B**) AFM images of the region 1 after 100-fold IPT.

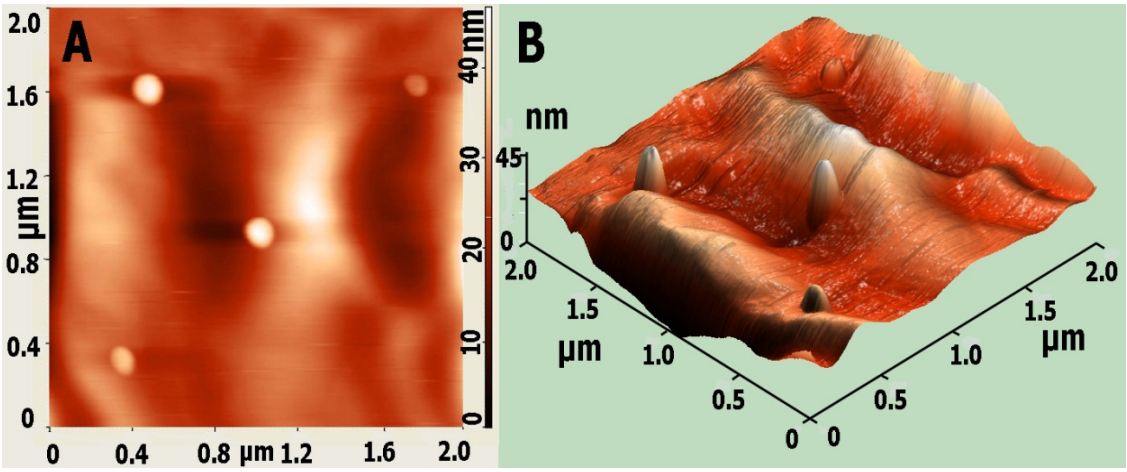

The conditions of appearance and the mechanism of development of surface pores and cones on a solid surface under ion bombardment have been studied in [57]. The author considered that ion-induced strains and deformations, initiating diffusion of atoms, displacement of dislocations and recrystallization in near-surface layers, are the main reasons for surface modification. Very probably the formation of pores occurs via supersaturation of the surface with interstitial atoms and by filling of the microscopic cavities in the crystal lattice. It generates open pores, firstly in the form of a ring with gradually increasing sidewall slope, and then stimulates the development of conical asperities at the bottom of the pores.

Under ion bombardment the redeposition of atoms from the sidewall to the bottom of the pores produces areas with lower stress level and, consequently, forms cones by means of local diffusion sinks. These conical formations lower strains at the bottom and the material flux towards the surface becomes smaller. As a result, the pore is decreased in size and then, it is sputtered [57].

Surfaces with such relief (Figure 20) can reveal reduced sputter and secondary electron yields. They have a low ion reflection coefficient and demonstrate selective optical properties and high field-emission characteristics. The structure of cones can change the catalytic, corrosion and emission

properties of the surface of contacts. One can see in Figure 21 (curve 1) that the stabilization of the breakdown voltage for samples with cone surface structures comes after 30 IPT cycles.

Figure 21. Median values of the breakdown voltage *U* (curve 1) and electrical resistance *R* (curve 2) of MKA-14108 reed switches versus the number *n* of IPT cycles. The sample set included 100 pieces.

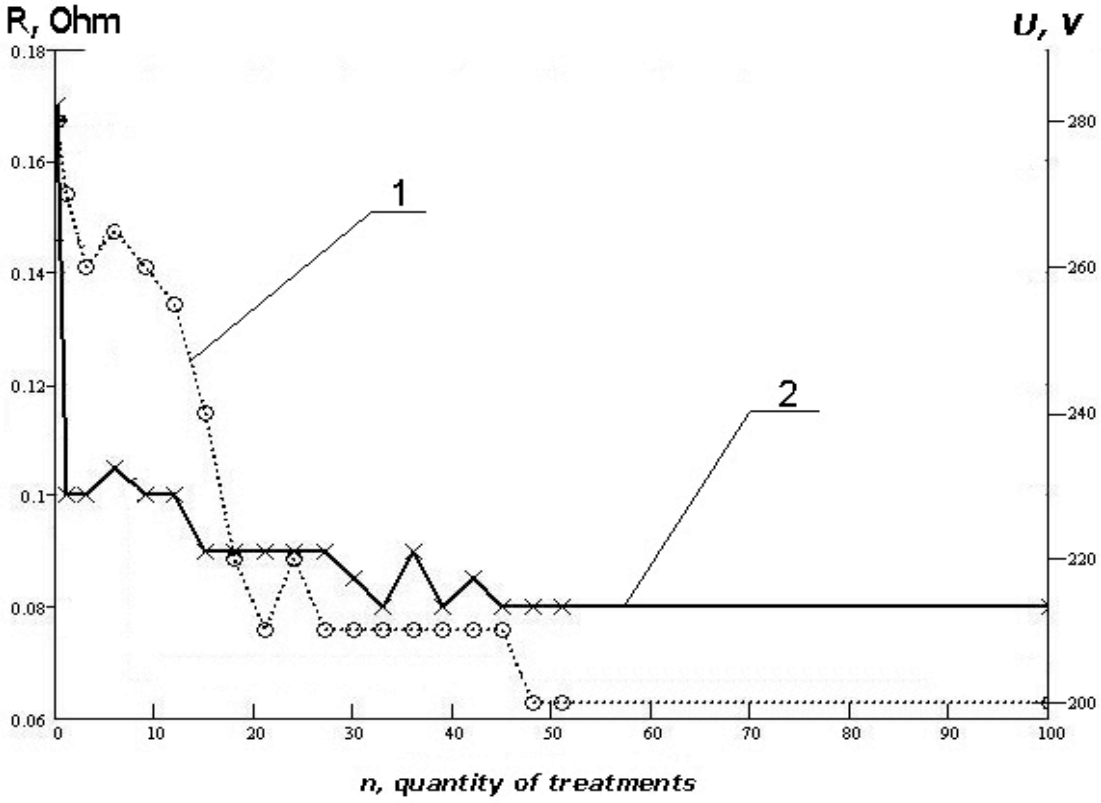

3.2.3. Potential Surface Relief

We used Kelvin probe force microscopy (KPFM) to observe the potential surface relief of contacts. From regions 1 to 3 the average surface potential exhibits small changes. For example, after 100-fold IPT, in the region 1 $\Delta\varphi_1 = -180$ mV (Figure 22) and in the region 2 $\Delta\varphi_2 = -100$ mV (Figure 23). After 10^7 cycles, the average potentials of all regions increase approximately by 130–160 mV (the work functions decrease by the same value). As-received samples (without IPT) have an average potential of 180 mV, it means that the work function of contacts after ion-plasma treatment grows by 0.36 eV due to the sputter cleaning and nitriding of their surfaces. These processes change the spreading of the electron cloud, which depends on surface relief and composition [28]. From Equation 28 one can see that the different spreading is the most probable reason for the differences in work function between as-received and treated samples.

Figure 22. 2D (**A**) and 3D (**B**) Kelvin probe force microscopy (KPFM) images of region 1 after 100-fold IPT.

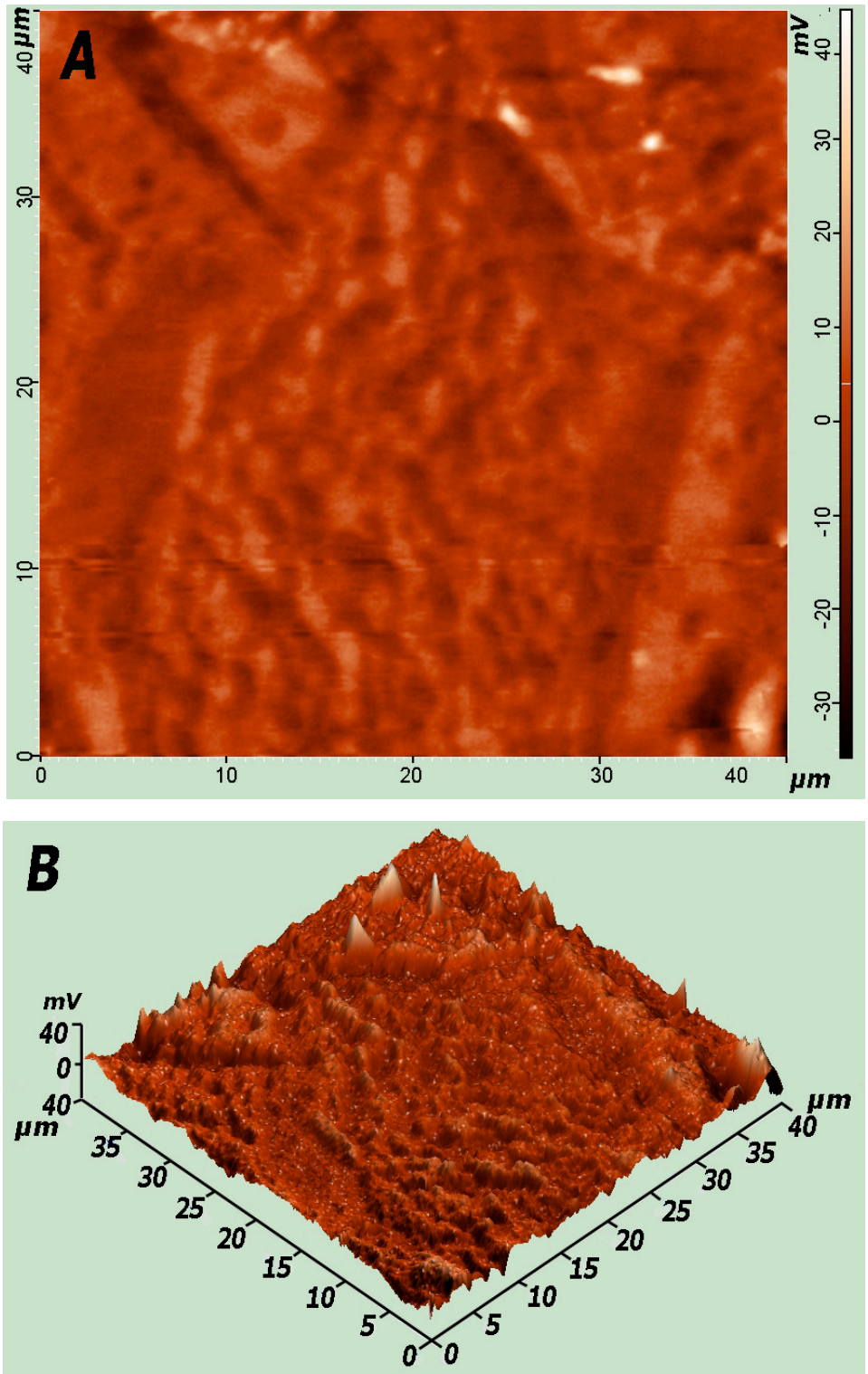

Figure 23. 2D (A) and 3D (**B**) KPFM images of the region 2 after 100-fold IPT.

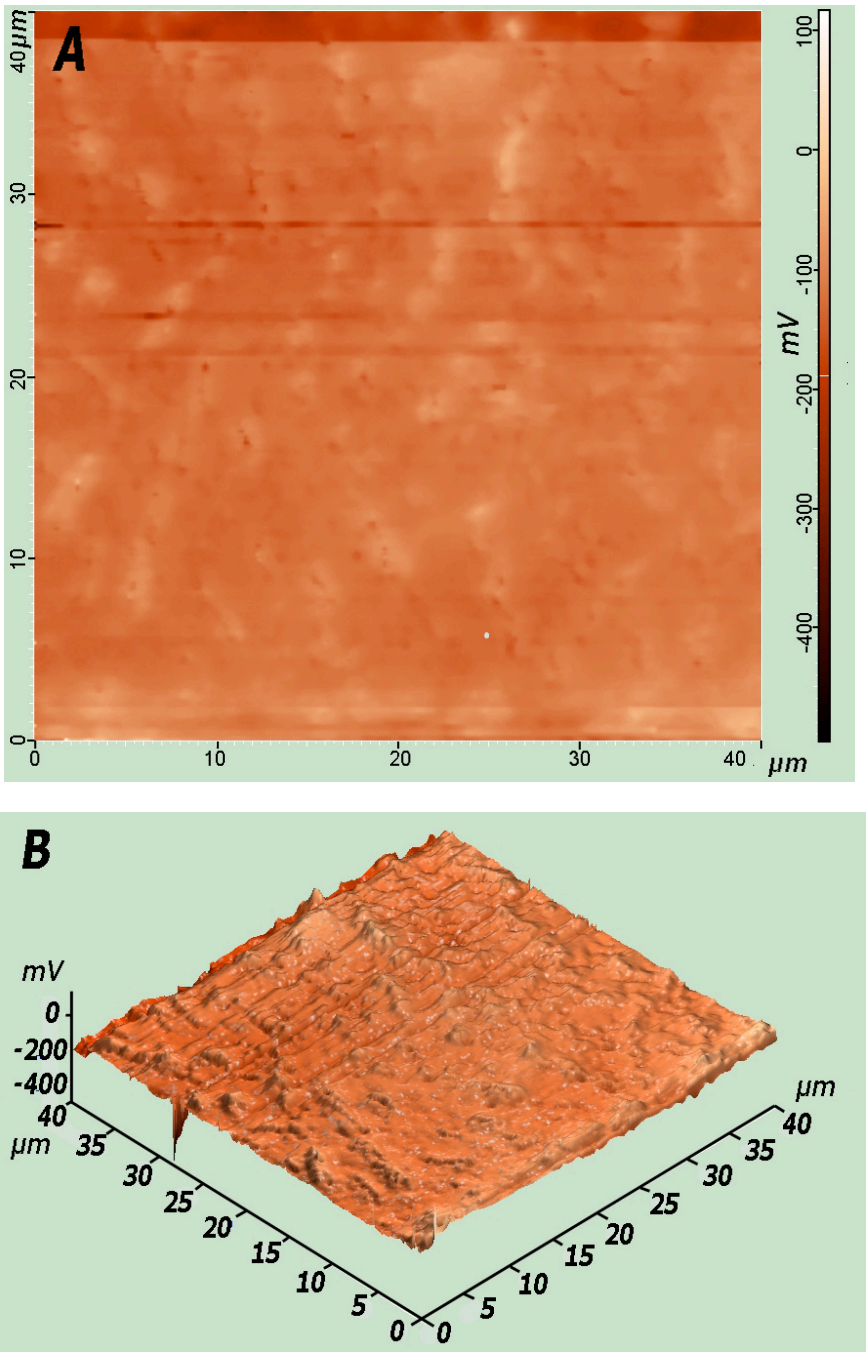

3.3. AES Diagnostics [58]

The results of AES analyses of contacts, information about manufacturing routes, IPT and switching conditions along with the data on resistance and breakdown voltage of reed switches are summarized in Table 2.

Table 2. Manufacturing route, IPT and switching conditions, resistance *R* and breakdown voltage *U*, elemental and chemical surface composition of the contacts estimated by Auger electron spectroscopy (AES).

Sample No.	Manufacturing route	IPT (Potential–Time–Number)	Switching	R (Ohm)	U (V)	Elemental composition	Chemical composition
1.6	Stamping, cleaning, annealing, sealing, IPT	200 V–30 s–50	10^7 cycles	0.09	240	Fe, Ni, C, N, O	$Fe_{3.3}N$, SiO_2 (out of IPT region)
57	Stamping, cleaning, annealing, etching, sealing, IPT	200 V–30 s–100	Without switching	0.1	200	Fe, Ni, C, N, O	$Fe_{3.3}N$, SiO_2 (out of IPT region)
14	Stamping, cleaning, annealing, sealing, IPT	200 V–30 s–100	Without switching	0.1	200	Fe, Ni, C, N, O,	$Fe_{3.3}N$, SiO_2 (out of IPT region)
1.1	Stamping, cleaning, annealing, sealing	Without IPT	Without switching	0.2	290	Fe, Ni, C, N, O, S, Cl	Iron and nickel oxides, SiO_2
1	Stamping, cleaning, annealing, sealing, IPT	200 V–30 s–1	Without switching	0.8	270	Fe, Ni, C, N, O	Fe_3N

Figure 24 shows the sputter depth profiles of sample 1 after one-fold IPT. The sputtering was carried out by 2.5 keV, 200 $\mu A \cdot cm^{-2}$ Ar^+ beam that provided a sputter rate of ca. 64 $nm \cdot min^{-1}$ for permalloy. Concentration, phase composition and thickness of the modified layer were estimated via measurements of the peak-to-peak amplitudes and some other features of Auger lines (for details, see [59] and references cited therein).

We found that in the depth between 14 and 26 nm and from 58 to 90 nm (Figure 24) nitrogen forms single-phase iron nitrides with a different concentration ratio C_{Fe}/C_N equal to 2.7 and 4.1, respectively.

The evaluated depth profiles of iron nitrides are shown in Figure 25. The near-surface region of the sample, about 14 nm in thickness, is greatly affected by surface contaminations and roughness along with the apparatus "crater effect", *i.e.*, nonuniform ion-beam etching over the crater's area. The deeper region (14–26 nm) exhibits a rather stable C_{Fe}/C_N ratio (2.7) with characteristic nitrogen Auger lines [60], and we identified the compound existing in this region as Fe_3N. Based upon the form of Auger lines and their chemical shifts, we decided that in the region situated between 58–90 nm the dominant compound is Fe_4N doped with oxygen and carbon impurities.

Figure 24. Evaluated concentration depth profiles of the main components and corresponding shape of nitrogen Auger lines representative for nitride phases of iron [60].

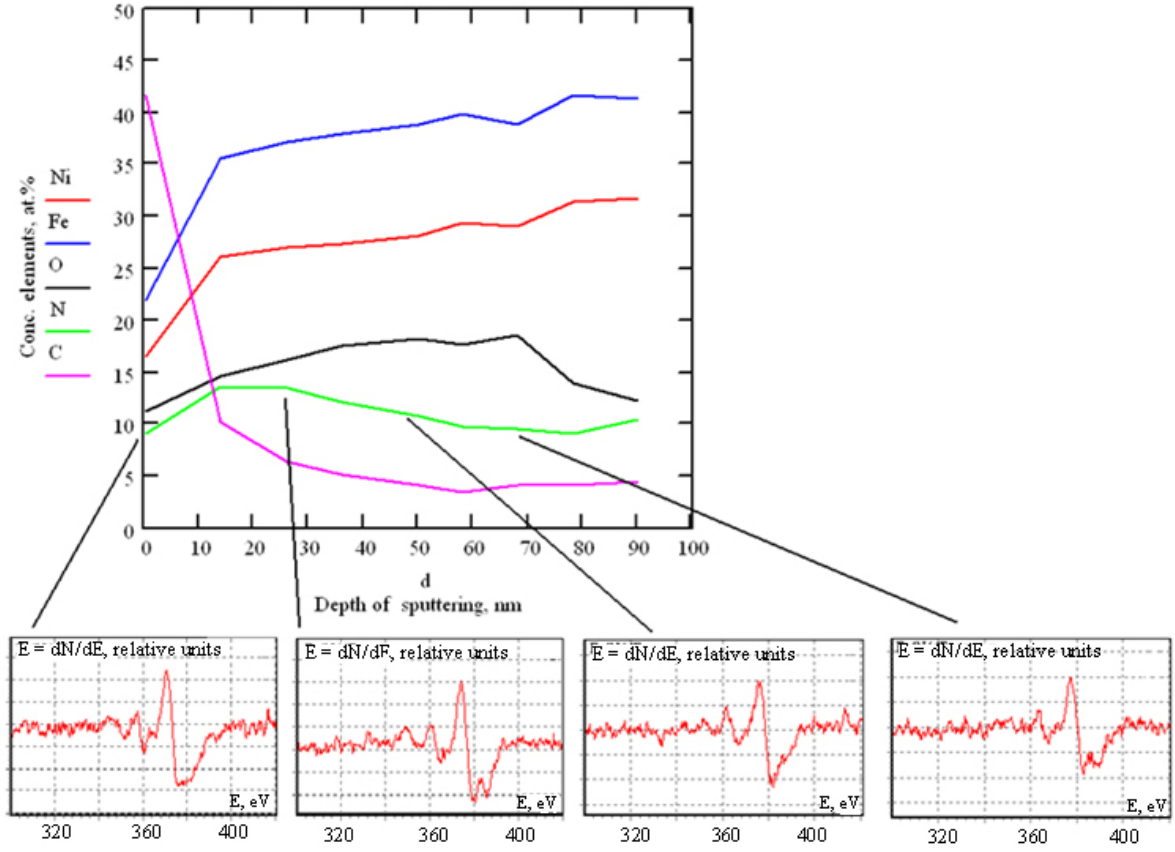

In sample 1.1, which was not subjected to ion-plasma treatment, we found the presence of SiO_2 over the overlapping zone of the contacts. At the same time, the characteristic nitride Auger lines were not registered for that sample.

For all other treated samples (see Table 2), we detected nitride Auger lines; and the SiO_2 concentration was found in negligible quantity in the overlapping zone. However, outside this zone glass impurities were also detected.

Depth profiling of samples 14 and 57, both after identical 100-fold IPT, revealed the presence of different iron nitrides. According to our estimate, $Fe_{3.3}N$ was found in the near-surface layers, and at a depth of ca.1 μm it was transformed into $Fe_{2.6}N$. Over all sputter depth we did not register any carbide compounds; the form of the carbon Auger line corresponds to the graphite phase only. In addition, sulphur with a bulk concentration of tenths of. % was found in sample 57.

In summary, using Auger electron spectroscopy, we detected on the surface of contacts, Fe_3N (after one-fold IPT) and $Fe_{3.3}N$ (after 30- and 100-fold IPT). These were transformed in deeper layers into Fe_4N (1-fold IPT) and $Fe_{2.6}N$ (30-, 100-fold IPT). Depending on the total duration of ion nitriding, the thickness of nitride layers was within the range from tens of nanometers (sample 1) to a few micrometers (samples 14 and 57).

Figure 25. Evaluated depth profiles of stoichiometric compounds Fe_3N and Fe_4N measured for sample 1.

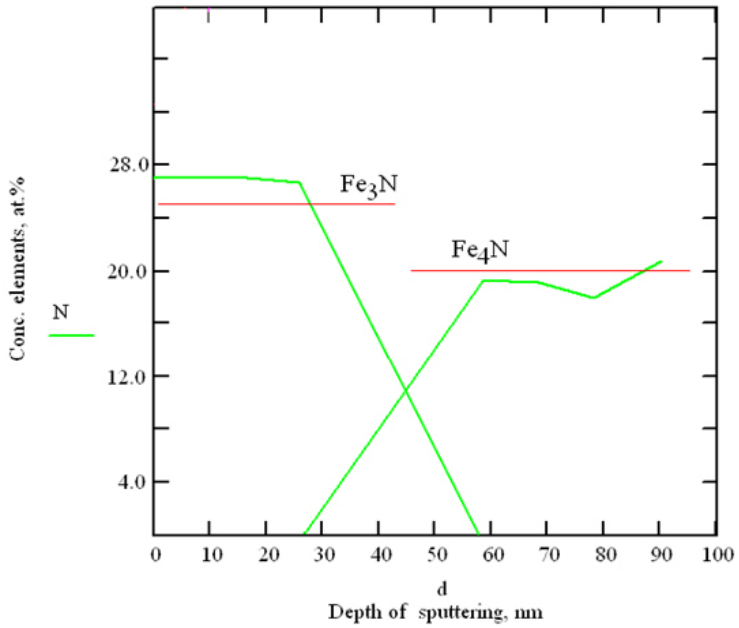

3.4. XPS Diagnostics [61]

Survey XPS spectra of samples 5, 14, 35 and 43 are presented in Figure 26 and Figure 27. The results of XPS data processing, resistance and breakdown voltage of reed switches are shown in Table 3.

The survey spectrum of sample 5 (Figure 26a) measured in the overlapping zone of the contacts after sealing the displays, besides iron and nickel lines, showed the presence of oxygen, carbon, silicon, fluorine and nitrogen. Detailed XPS spectra **(**not shown here**)** indicate that Fe and Ni are oxidized. The main peak of nitrogen N 1s (397.3 eV) along with the peak Si 2p (102.5 eV) is a strong point for the presence of Si_3N_4.

From the data shown in Figure 26, Figure 27 and in Table 3 we suppose that the growth of reed switch resistance, after sealing, is caused by oxidation of the surface of the contacts, deposition of glass particles and some products of glass thermal decomposition along with chemical residues (e.g., the components of hydrofluoric acid used for manufacturing of glass envelopes), adsorption of vacuum oil vapors, *etc*.

After 30-fold IPT (samples 14, 43 and 52 in Table 3) the resistance decreased and became the same as the resistance of commercially produced MKA-14103 reed switches.

Figure 26. Survey XPS spectra measured for the samples 5 (**A**) and 14 (**B**).

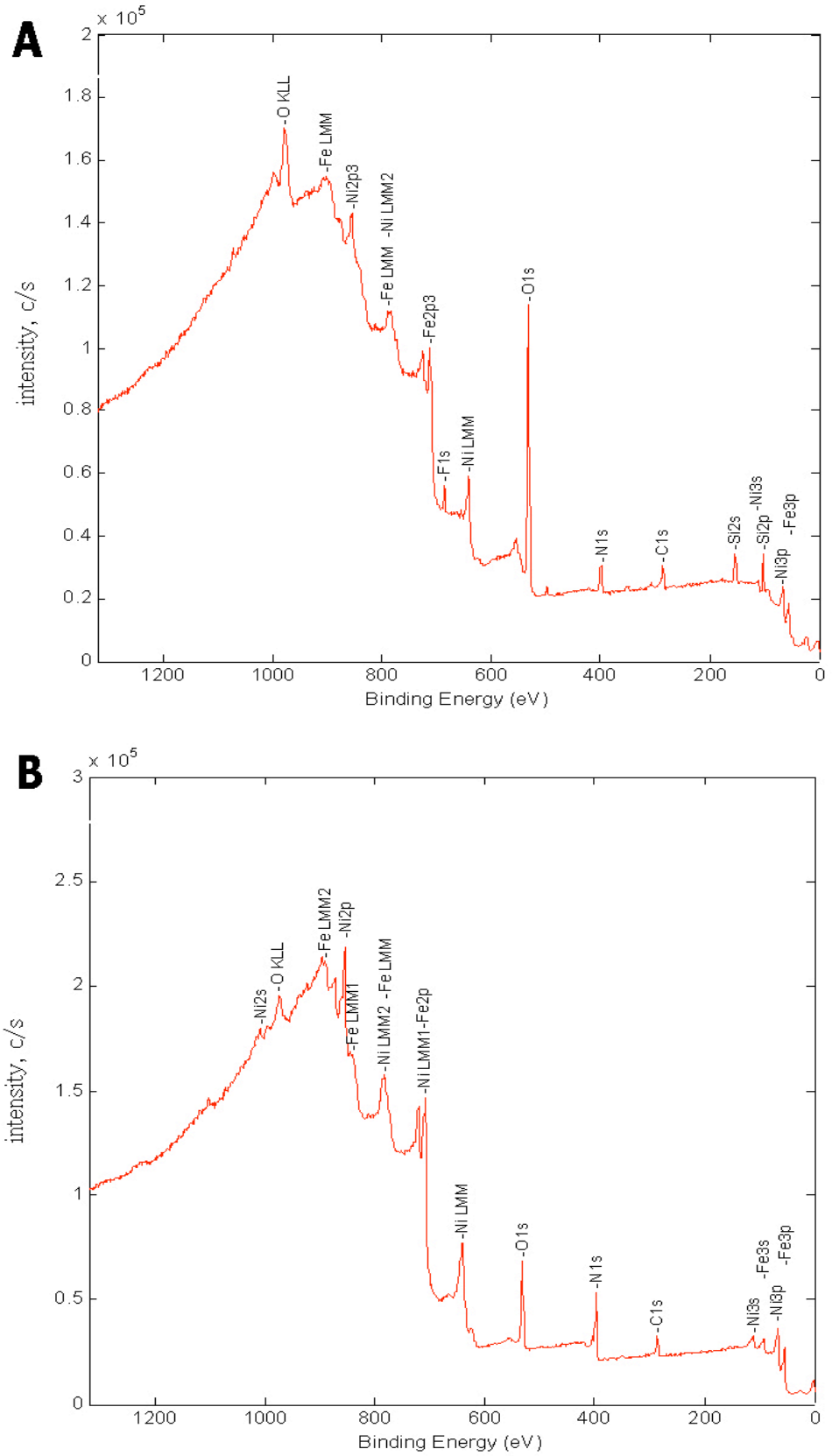

Figure 27. Survey X-ray photoelectron spectroscopy (XPS) spectra measured for samples 35 (**A**) and 43 (**B**).

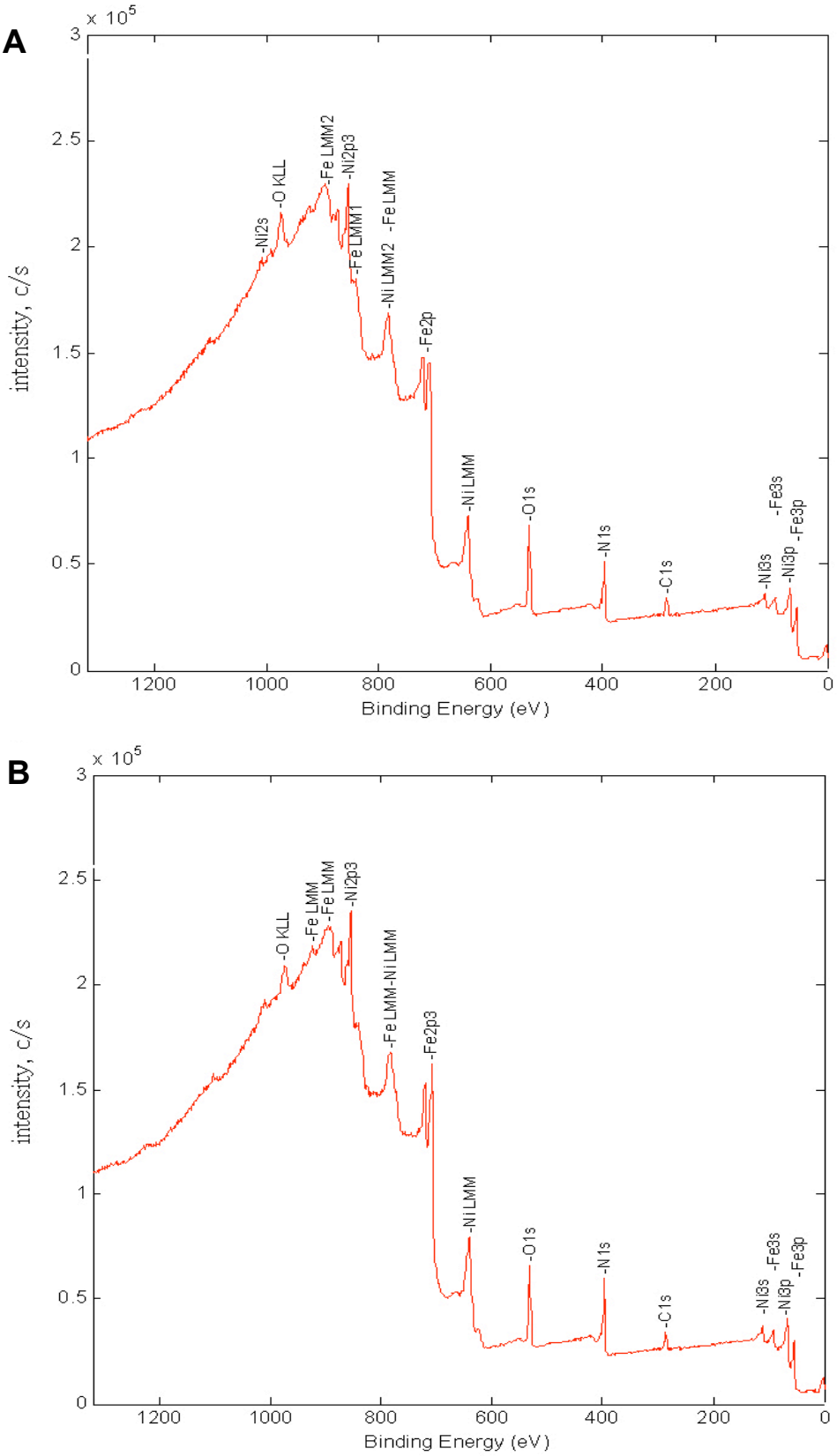

Table 3. IPT and switching conditions, resistance *R* and breakdown voltage *U*, elemental surface composition of the contacts measured by X-ray photoelectron spectroscopy (XPS).

Sample No.	IPT (Potential–Time–Number)	Switching (Potential–Current–Number of cycles–Temperature)	R (Ohm)	U (V)	Elemental concentration (at. %)						
					C1s	N1s	O1s	Fe2p	Ni2p	F1s	Si2p
35	200 V–30 s–100	Without switching	0.08	210	13.5	29.2	27.6	17.8	11.9	-	-
43	200 V–30 s–30	Without switching	0.09	200	13.4	31.6	22.4	18.5	14.1	-	-
52	200 V–30 s–30	30 V–0.5 A–1.25×10^6 at 155 ºC, and 1.25×10^6 at RT	0.09	250	22.4	27.6	26.0	13.9	10.1	-	-
14	200 V–30 s –30	50 mV–5 μA–10^8 at RT	0.09	220	14.5	30.5	24.7	16.8	13.5	-	-
5	Without IPT	Without switching	0.22	290	9.3	8.7	53.5	8.3	4.6	3.3	12.5

The survey spectrum of sample 43 (Figure 27b), obtained after 30-fold IPT, shows lines of iron, nickel, oxygen, carbon, and nitrogen. However, as opposed to the data presented in Figure 26a for sample 5 (without IPT), Si and F lines have disappeared, the intensity of O is reduced, and Fe, Ni, N and C have become more intense. We put down all these changes, including the decrease of resistance and breakdown voltage of ion-plasma treated reed switches, to the erosion of polymer films and surface oxides layers by nitrogen ion bombardment together with surface nitriding and gettering processes.

Detailed XPS spectra (not shown here) demonstrate the shift of the Ni 2p line towards greater binding energy due to the formation of nitride or oxynitride phases. The line with 707.5 eV in the Fe 2p spectrum corresponds to the nitride phase as well as the main peak of N 1s (397.3 eV).

Long-duration IPT (sample 35 after 100-fold treatment) gives approximately the same results as shorter treatment (see Table 3 and survey spectra presented in Figure 27).

After the low-power switching test (sample 14), the intensity of C and O lines increased and, conversely, the lines of Fe, Ni and N exhibited a small decrease (Table 3). The results obtained after the high-power test (sample 52) confirm this tendency, but both increasing and decreasing of the lines intensity were more pronounced (Table 3) due to plasma arc formation during contact breaking [1]. Such arc can locally heat the surface of the contacts and evaporate the permalloy components. As a result, spot craters of ca. 2 μm in diameter and 100–150 nm in depth are formed.

Simultaneously, the diffusion release of carbon and oxygen from the bulk of contacts is activated and according to our mass spectrometric measurements leads to intense CO_2 production. In the heated spots, surface nitride compounds decomposed and emitted nitrogen. The breakdown voltage grows by 50 V. However, in spite of partial damaging of the nitride layers, both under the low- and high-power switching tests, the number of reed switch failures does not increase.

4. Conclusions

Our developments and research in the field of ion-induced surface modification of magnetically operated contacts (reed switches) are summarized in this paper.

We proposed to produce nano- and micro-sized nitride layers on the surface of permalloy contacts directly into reed switches after sealing, by means of glow-discharge nitrogen plasma initiated with high voltage pulses supplied to open contacts. Based on the results of thorough experimental studies, we have chosen optimal discharge conditions for providing the formation of corrosion- and erosion-resistant iron and nickel nitride coatings, with high electrical conductivity and adhesive ability via ion nitriding and reactive cathode sputtering of the near-surface layers of the contacts. It allows reducing, and in the near future complete abandoning, of the electrodeposition of precious and high-cost metals in the commercial manufacture of reed switches.

Conflict of Interest

Partly presented in Russian at the 3rd International Scientific and Practical Conference on Reed Switches and Reed Switches Based Products (ICRS–2011), Ryazan (Russian Federation), 28–30 September 2011.

Acknowledgments

We are very grateful to A.A. Kuznetsov for performing AES surface and sputter depth profiling of contacts and A.V. Naumkin for XPS measurements.

References

1. Karabanov, S.M.; Maizels, R.M.; Shoffa, V.N. *Magnetically Operated Contacts (Reed Switches) and Products on Their Basis* [Russian]; Intellekt: Dolgoprudnyi, Russia, 2011; p.150.
2. Arzamasov, B.N.; Bratuchin, A.G.; Eliseev, Y.S.; Panayoty, T.A. *Ion Chemical-Thermal Surface Machining of Alloys in Gas Environment* [Russian]; BMSTU: Moscow, Russia, 1999; p. 96.
3. Lyaszcenko, B.A.; Mironenko, V.I.; Rad'ko, O.V.; Bobyr', S.A. Nitriding of 30KHGSA steel in pulsing discharge. *Vestnik Cherkasskogo Natsional'nogo Universiteta* **2007**, *117*, 107–110.
4. Zeltser, I.A.; Karabanov, S.M.; Maizels, R.M.; Sablin, V.A. Modification of the surface of sealed magnetically operated permalloy contacts by means of pulsing glow-discharge [Russian]. In *Proceedings of the 2nd International Scientific and Practical Conference on Magnetically Operated Contacts (Reed Switches) and Reed Switches Based Products (ICRS–2008)*, Ryazan, Russia, 1–3 October 2008; pp. 174–177.
5. Zeltser, I.A.; Karabanov, S.M.; Maizels, R.M.; Sablin, V.A. Investigation and development of surface modification methods for magnetically operated contacts [Russian]. In *Proceedings of the 2nd International Scientific and Practical Conference on Magnetically Operated Contacts (Reed Switches) and Reed Switches Based Products (ICRS–2008)*, Ryazan, Russia, 1–3 October 2008; pp. 184–207.

6. Zeltser, I.A.; Karabanov, S.M; Kuznetsov, A.A.; Maizels, R.M.; Sablin, V.A.; Chernyak, E.Y. Study on ion-plasma modification of iron-nickel contacts by Auger electron spectroscopy [Russian]. In *Proceedings of the 2nd International Scientific and Practical Conference on Magnetically Operated Contacts (Reed Switches) and Reed Switches Based Products (ICRS–2008)*, Ryazan, Russia, 1–3 October 2008; pp. 178–183.
7. Karpov, A.S.; Maizels, R.M.; Shishkina, L.V.; Shkutenko, L.N. Plant for automatic ion-plasma treatment of reed switches [Russian]. In *Proceedings of the 2nd International Scientific and Practical Conference on Magnetically Operated Contacts (Reed Switches) and Reed Switches Based Products (ICRS–2008)*, Ryazan, Russia, 1–3 October 2008; pp. 169–173.
8. Kuznetsov, A.A.; Vasiliev, E.V.; Zeltser, I.A.; Chernyak, E.Y. AES analysis of elemental and chemical composition of reed switches [Russian]. In *Proceedings of the 2nd International Scientific and Practical Conference on Magnetically Operated Contacts (Reed Switches) and Reed Switches Based Products (ICRS–2008)*, Ryazan, Russia, 1–3 October 2008; pp. 84–87.
9. Arushanov, K.A.; Zeltser, I.A. Instrumental and technological features of reed switch production with nanostructured contact surfaces [Russian]. *Vestnik RGRTU* **2009**, *3*, 93–98.
10. Zeltser, I.A.; Karabanov, S.M.; Maizels, R.M.; Moos, E.N.; Sablin, V.A. Surface modification of magnetically operated nickel-iron contacts [Russian]. In *Abstracts of the Proceedings of the 10th International Seminar on Materials Modification using Modern Alternative Technologies*, Obninsk, Russia, 10–12 September 2009; pp. 58–59.
11. Zeltser, I.A.; Karabanov, S.M.; Maizels, R.M.; Moos, E.N.; Sablin, V.A. Nanostructure Modificated Contact Surface. In *Abstracts of the International Conference on Information and Structure in Nanoworld*, Saint-Petersburg, Russia, 1–3 July 2009; p. 83.
12. Karabanov, S.M.; Zeltser, I.A.; Maizels, R.M.; Trunin, E.B. Magnetically operated sealed contact. RF Patent 2 391 733, 2 September 2008.
13. Karabanov, S.M.; Maizels, R.M.; Arushanov, K.A.; Zeltser, I.A.; Provotorov, V.S. Method of producing reed switches with nitrided contacts. RF Patent 2 393 570, 18 June 2009.
14. Arushanov, K.A.; Zeltser, I.A.; Karabanov, S.M.; Maslakov, K.I.; Naumkin, A.V. Study on plasma modification of magnetically operated contacts by X-ray photoelectron spectroscopy and atomic force microscopy [Russian]. In *Proceedings of the 7th International Science and Practical Conference on New Progress of European Science*; Sofia, Bulgaria, 23–26 June 2011; Volume 36, pp. 56–61.
15. Arushanov, K.A.; Zeltser, I.A.; Karabanov, S.M.; Maizels, R.M.; Moos, E.N. New method of modification of the contact surfaces of reed switches [Russian]. In *Proceedings of the 7th International Science and Practical Conference on New Progress of European Science*, Sofia, Bulgaria, 23–26 June 2011; Volume 36, pp. 52–55
16. Arushanov, K.A.; Zeltser, I.A.; Karabanov, S.M.; Maizels, R.M.; Moos, E.N. Formation of the nano-relief of contact surfaces [Russian]. In *Abstracts of the 11th International Seminar on Materials Modification*; Obninsk, Russia, 15–16 May 2011; pp. 20–22.
17. Arushanov, K.A.; Zeltser, I.A.; Karabanov, S.M.; Maizels, R.M.; Moos, E.N. Ion-induced modification of contact surfaces [Russian]. In *Proceedings of the 20th International Conference on Ion Interaction with Surface* (*ISI-2011)*, Zvenigorod, Russia, 2011; pp. 206–209.

18. Arushanov, K.A.; Zeltser, I.A.; Karabanov, S.M.; Trunin, E.B. Diffusion saturation of near-surface layers of reed switch by nitrogen in pulsing plasma [Russian]. In *Abstracts of the 3th International Scientific and Practical Conference on Magnetically Operated Contacts (Reed Switches) and Reed Switches Based Products (ICRS–2011)*, Ryazan, Russia, 28–30 September 2011; pp. 31–38.
19. Avachev, A.P.; Arushanov, K.A.; Zeltser, I.A.; Karabanov, S.M.; Konobeev, V.A. Study on plasma modification of magnetically operated contacts by atomic force and optical microscopy [Russian]. In *Abstracts of the 3th International Scientific and Practical Conference on Magnetically Operated Contacts (Reed Switches) and Reed Switches Based Products (ICRS–2011)*, Ryazan, Russia, 28–30 September 2011; pp. 47–53.
20. Arushanov, K.A.; Zeltser, I.A.; Karabanov, S.M.; Maizels, R.M.; Moos, E.N. A novel method of surface modification of magnetically operated contacts [Russian]. In *Abstracts of the 3th International Scientific and Practical Conference on Magnetically Operated Contacts (Reed Switches) and Reed Switches Based Products (ICRS–2011)*, Ryazan, Russia, 28–30 September 2011; pp. 54–60.
21. Arushanov, K.A.; Zeltser, I.A.; Karabanov, S.M.; Maslakov, K.I.; Naumkin, A.V. Study on ion-plasma modification of iron-nickel contacts by X-ray photoelectron spectroscopy [Russian]. In *Abstracts of the 3th International Scientific and Practical Conference on Magnetically Operated Contacts (Reed Switches) and Reed Switches Based Products (ICRS–2011)*, Ryazan, Russia, 28–30 September 2011; pp. 39–46.
22. Zhuravlev, S.A.; Zeltser, I.A.; Maizels, R.M.; Polyakov, A.S.; Chernyak, E.Y. Gas analysis inside reed switches [Russian]. In *Abstracts of the 3th International Scientific and Practical Conference on Magnetically Operated Contacts (Reed Switches) and Reed Switches Based Products (ICRS–2011)*, Ryazan, Russia, 28–30 September 2011; pp. 68–69.
23. Arushanov, K.A.; Zeltser, I.A.; Kuznetsov, A.A.; Chernyak, E.Y. Application of Auger electron spectroscopy for study of plasma modification of magnetically operated contacts [Russian]. In *Abstracts of the 3th International Scientific and Practical Conference on Magnetically Operated Contacts (Reed Switches) and Reed Switches Based Products (ICRS–2011)*, Ryazan, Russia, 28–30 September 2011; pp. 61–67.
24. Drozdov, M.N.; Zeltser, I.A.; Karabanov, S.M.; Teodoro O.M.N.D.; Tolstoguzov A.B. Study on ion-plasma modification of magnetically operated contacts by secondary ion mass spectrometry [Russian]. In *Abstracts of the 3th International Scientific and Practical Conference on Magnetically Operated Contacts (Reed Switches) and Reed Switches Based Products (ICRS–2011)*, Ryazan, Russia, 28–30 September 2011; pp. 129–133.
25. Karabanov, S.M.; Zeltser, I.A.; Maizels, R.M.; Moos, E.N.; Arushanov, K.A. Creation of principally new generation of switching technique elements (reed switches) with nanostructured contact surfaces. *J. Phys.: Conference Ser.* **2011**, *291*, 1–17.
26. Chatterjee-Fischer, R.; Eysell F.-W; Lidke D. *Nitriding and Carbonitriding* [Russian]; Metallurgiya: Moscow, Russia, 1990; p. 278.
27. Systat Software Inc. SigmaPlot 12. Available online: http://www.sigmaplot.com (accessed on 17 February 2012).

28. Solomin, Y.M. Magnetically operated contacts [Russian]. *Elektronnaya Tekhnika (Ser. 4)* **1975**, *7*, 23–28.
29. Shuppe, G.N. *Electron and Ion Emissions. Basic Physics for Electronic Engineering, Part 2* [Russian]; RRTI: Ryazan, Russia, 1986; p. 84.
30. Feynman, R.; Leyton, R.; Sands, M. *Electricity and Magnetism. Feynman's Lectures on Physics* [Russian], 5th ed.; Mir: Moscow, Russia, 1967; p. 273.
31. Dekhtyar, I.Y. Defects of the crystalline structure and some properties of metals and alloys [Russian]. *Uspekhi Fiz. Nauk* **1957**, *62*, 99–128.
32. Starenchenko, V.A.; Cherepanov, D.N.; Solovieva, Y.V.; Popov, L.E. Generation and accumulation of the point defects during plastic deformation in single crystals with fcc structure [Russian]. *Izvestiya Vuzov. Fiz.* **2009**, *4*, 60–71.
33. Gufrein, N.S.; Dobytchin, D.R.; Konlenko, L.S. Calculation of the increasing adsorption energy in molecular dimensions pores for nonspecific nonlocalized adsorption [Russian]. *Zh. Fiz. Khimii* **1970**, *44*, 741–747.
34. Lozovik, Y.E.; Popov, A.M. Formation of carbon nanoparticles in electric arc [Russian]. *Teplofiz.Vysokikh Temperatur* **1995**, *33*, 539–543.
35. Lozovik, Y.E.; Popov, A.M. Formation and growth of carbon nanostructures—Fullerenes, nanoparticles, nanotubes and cones [Russian]. *Uspekhi Fiz. Nauk* **1997**, *167*, 751–760.
36. Bogomolov, R.M.; Krylov, S.M.; Gromakovsky, D.G.; Ibatullin, I.D. Hardening of surface layers via diffusion molecular reinforcement [Russian]. *Trenie*, *Iznos*, *Smazka* **2007**, *9*, 12–17.
37. Lazarev, S.D.; Babulevich, N.E.; Varfolomeev, A.E. Sensor diagnostics of mechanical condition of solid-state materials [Russian]. *Zh.Tekh. Fiz.* **2000**, *70*, 106–110.
38. Merl, V. *Electric Contact* [Russian]; GEI: Moscow, Russia, 1962; p. 490.
39. Holm, R. *Electric Contacts Handbook*; Springer-Verlag: Berlin, Germany, 1958; p. 433.
40. Rakhovsky, V.I. *Basic Physics of Switching of Electric Current in Vacuum* [Russian]; Nauka: Moscow, Russia, 1970; p. 378.
41. Mesyats, G.A. Ecton or electron avalanche of metal [Russian]. *Uspekhi Fiz. Nauk* **1995,** *165*, 601–611.
42. Zeltser, I.A.; Kukushkin, S.A.; Sablin, V.A.; Moos, E.N. Material modification using alternative technologies [Russian]. In *Abstracts of the Reports (MNT-IX)*, Obninsk, Russia, 2007; p. 38.
43. Zeltser, I.A.; Moos, E.N.; Sablin, V.A.; Trunin, E.B. Magnetically operated contacts (reed switches) and products on their basis [Russian]. In *Proceedings of the 2nd International Scientific and Practical Conference on Magnetically Operated Contacts (Reed Switches) and Reed Switches Based Products (ICRS–2008)*, Ryazan, Russia, 1–3 October 2008; pp. 111–122.
44. Dedkov, G.V. Nanotribology: Experimentals and theoretical models [Russian]. *Uspekhi Fiz. Nauk* **2000**, *170*, 585–618.
45. Kolesnikov, V.I.; Bulgarevich, S.B.; Kozakov, A.T.; Sidashov, A.V.; Boyko, M.V. Experimental and theoretical investigations of segregation on connected surfaces and intercrystalline boundaries of materials in tribosystem "wheel-rail-brake" [Russian]. *Vestnik YUNTS RAN* **2007**, *3*, 9–20.
46. Gritsenko, B.P.; Krukovsky, K.V.; Girsova, N.V.; Kashin, O.A. An influence of high-dose ion implantation and acoustic vibrations generated under friction on wear resistance of armco iron and steel 45 [Russian]. *Trenie i Iznos* **2005**, 2*6*, 593–599.

47. Gritsenko, B.P.; Kashin, O.A. An influence of high-dose ion implantation and acoustic vibrations on deformation and wear resistance of steel 45 [Russian]. *Izvestiya Tomskogo Politekhnicheskogo Universiteta* **2004**, *307*, 121–125.
48. Gritsenko, B.P.; Krukovsky, K.V.; Kashin, O.A. Deformation behavior of ion-implanted armco iron and steel 45 under friction and wear with damping of acoustic oscillations [Russian]. *Fiz. Mezomekhanika* **2004**, *7*, 415–418.
49. Sharkeev, Yu.P.; Perry, A.J.; Gritsenko, B.P.; Fortuna, S.V. Modification of metallic materials and hard coatings using vacuum arc metal ion implantation. *Vacuum* **1999**, *52*, 247–254.
50. Girsova, N.V.; Gritsenko, B.P.; Sharkeev, Y.P.; Ryabchikov, A.I.; Tailashev, A.S.; Fortuna, A.S.; Kozlov, E.V. Structure and phase transformations in alloy Fe_3N at high-dose ion implantation [Russian]. *Izvestiya Vuzov. Fiz.* **1998**, *11*, 15–24.
51. Gritsenko, B.P. Role of acoustic vibrations generated under friction in destruction of tribosystem materials [Russian]. *Trenie i Iznos* **2005**, *26*, 481–488.
52. Sharkeev, Yu.P.; Gritsenko, B.P.; Fortuna, S.V.; Perry, A.J. Modification of metals and hard coatings using vacuum-arc metal ion implantation. In *Ion Implantation Technology*; IEEE: Piscataway, N.J., USA, 1999; pp. 873–876.
53. Gritsenko, B.P.; Bespalov, V.V. An influence of modification of the near-surface layers of materials on wear resistance in tribological pairs [Russian]. In *Proceedings of the 6th International Conference on Modifications of Materials with paRticle Beams and Plasma Flows*, Tomsk, Russia, 23–28 September 2002; pp. 432–434.
54. Gan, Y. Atomic and subnanometer resolution in ambient conditions by atomic force microscopy. *Surf. Sci. Rep.* **2009**, *64*, 99–121.
55. Zeltser, I.A.; Karabanov, S.M.; Moos, E.N. Formation of the dissipative structures in crystals at thermal transfer and electric transport [Russian]. *Fiz. Tverdogo Tela* **2005**, *47*, 1921–1926.
56. Emelyanov, V.I.; Rukhlyada, N.Y. Defect induced instability and formation of two-dimensional surface structures by plasma surface treatment [Russian]. *Naukoemkie Tekhnologii* **2009**, *10*, 3–13.
57. Begrambekov, L.B. *Modification of Solid Surface under Ion and Plasma Irradiation* [Russian]; MIFI: Moscow, Russia, 2001; p. 34.
58. Davies, L.E., Mac Donald, N.C., Palmberg, P.W., Riach, G.E., Weber, R.E. *Handbook of Auger Electron Spectroscopy*, 2nd ed.; Perkin Elmer Corp., Phys. Electronic Div.: Eden Prairie, MN, USA, 1976; p. 450.
59. Kuznetsov, A.A.; Abramova, S.Yu.; Potapova, T.E.; Protopopov, O.D. AES and LEED studies of surface stoichiometry of palladium silicide epilayers on Si (111). *J. Electron Spectr. Rel. Phenom.* **1994**, *68*, 407–412.
60. Vanden Berghe, R.; Vlaeminck, R. On the N KLL spectra of some nitrides. *Surf. Interface Anal.* **1987,** *10*, 316–318.

61. Briggs, D.; Seah, M.P. *Practical Surface Analysis by Auger and X-ray Photoelectron Spectroscopy*, 2nd ed.; John Wiley: Chichester, UK, 1990; p. 658.